

ESTIMATING A COMMON COVARIANCE MATRIX FOR NETWORK META-ANALYSIS OF GENE EXPRESSION DATASETS IN DIFFUSE LARGE B-CELL LYMPHOMA*

BY ANDERS ELLERN BILGRAU^{†,‡,§}, RASMUS FROBERG BRØNDUM^{‡,§},
POUL SVANTE ERIKSEN[†], KAREN DYBKÆR[‡], AND MARTIN
BØGSTED^{†,‡}

*Aalborg University[†] and Aalborg University Hospital[‡]
Shared first authorship[§]*

The estimation of covariance matrices of gene expressions has many applications in cancer systems biology. Many gene expression studies, however, are hampered by low sample size and it has therefore become popular to increase sample size by collecting gene expression data across studies. Motivated by the traditional meta-analysis using random effects models, we present a hierarchical random covariance model and use it for the meta-analysis of gene correlation networks across 11 large-scale gene expression studies of diffuse large B-cell lymphoma (DLBCL). We suggest to use a maximum likelihood estimator for the underlying common covariance matrix and introduce an EM algorithm for estimation. By simulation experiments comparing the estimated covariance matrices by cophenetic correlation and Kullback-Leibler divergence the suggested estimator showed to perform better or not worse than a simple pooled estimator. In a posthoc analysis of the estimated common covariance matrix for the DLBCL data we were able to identify novel biologically meaningful gene correlation networks with eigengenes of prognostic value. In conclusion, the method seems to provide a generally applicable framework for meta-analysis, when multiple features are measured and believed to share a common covariance matrix obscured by study dependent noise.

1. Introduction. Human cells carry out their function in concerted interaction via intricate protein signalling networks. These networks are according to the central dogma of molecular biology controlled by expressed genes. It has become popular to perform genome wide measurements of expressed genes and proteins and summarizing the information by huge covariance matrices leading to improved understanding of disease pathology and identification of new drug targets (Agnelli et al., 2011; Clarke et al., 2013).

*Supported by MSCNET, EU FP6, CHEPRE, the Danish Agency for Science, Technology, and Innovation as well as Karen Elise Jensen Fonden.

Keywords and phrases: covariance estimation, precision estimation, integrative analysis, meta-analysis, network analysis

Many gene expression studies, however, are hampered by low sample size and it has therefore become of interest to increase sample size by collecting gene expression data across studies. These data are potentially hampered by severe batch effects, and robust methods are therefore required to conduct meta-analysis of covariance matrices.

To the best of our knowledge no approaches exist where meta-analysis of covariance matrices have been addressed explicitly. We acknowledge, however, that a number of indirect methods have been constructed. An immediate and tempting approach is to use one of the many study correcting approaches scattered around in the literature (Irizarry et al., 2003; Johnson, Li and Rabinovic, 2007; Lee, Dobbin and Ahn, 2014) followed by estimating the covariance matrix either based on a pooled data set or by pooling covariance matrices estimated from each individual study as suggested by Lee, Dobbin and Ahn (2014). This approach, however, suffers from the same disadvantages as usual meta-analysis based on pooling fixed effects as it puts too much weight on large outliers in the data (Borenstein et al., 2010).

Motivated by the alternative meta-analysis by random effects (DerSimonian and Laird, 1986; Choi et al., 2003), we suggest a hierarchical model where the covariance for each study is assumed to be drawn from an inverse Wishart distribution with a common mean covariance matrix, and data from each study is then subsequently generated from a multivariate Gaussian distribution with this covariance matrix. We suggest to use a maximum likelihood estimator for the underlying common covariance matrix and introduce an EM algorithm for its estimation. We use the method for the meta-analysis of gene correlation networks across 11 large-scale gene expression studies of diffuse large B-cell lymphoma (DLBCL). It is our expectation that a more suitable handling of the covariance matrix will lead to more adequate estimations of covariance matrices and subsequently inferred gene correlation networks.

In Section 2, we propose the model for a common covariance matrix across multiple studies, derive estimators thereof, and propose an inter-study homogeneity measure to aid in assessing the variation between studies. We conduct an extensive simulation study in Section 3 comparing the proposed estimator and simple pooling of covariance matrices. We then apply the model in Section 4 to 2,046 DLBCL samples across 11 datasets before concluding the manuscript in Section 5.

2. A hierarchical model for the covariance matrix. Let p be the number of features and k the number of studies. We model an observation \mathbf{x} from the i 'th study as a p -dimensional zero-mean multivariate Gaussian

vector with covariance matrix realized from an inverse Wishart distribution, i.e. \mathbf{x} follows the hierarchical model

$$(2.1) \quad \begin{aligned} \boldsymbol{\Sigma}_i &\sim \mathcal{W}_p^{-1}(\boldsymbol{\Psi}, \nu), \\ \mathbf{x}|\boldsymbol{\Sigma}_i &\sim \mathcal{N}_p(\mathbf{0}_p, \boldsymbol{\Sigma}_i), \quad i = 1, \dots, k, \end{aligned}$$

where $\mathcal{N}_p(\boldsymbol{\mu}, \boldsymbol{\Sigma}_i)$ denotes a p -dimensional multivariate Gaussian distribution with mean $\boldsymbol{\mu}$ and positive definite (p.d.) covariance matrix $\boldsymbol{\Sigma}_i$, and probability density function (pdf) shown in (B.1), and $\mathcal{W}_p^{-1}(\boldsymbol{\Psi}, \nu)$ denotes a p -dimensional inverse Wishart distribution with $\nu > p - 1$ degrees of freedom, a p.d. $p \times p$ scale matrix $\boldsymbol{\Psi}$, and pdf shown in (B.2). While the inverse Wishart distribution is defined for all $\nu > p - 1$, the first order moment exists only when $\nu > p + 1$ and is given by

$$(2.2) \quad \mathbb{E}[\boldsymbol{\Sigma}_i] = \boldsymbol{\Sigma} = \frac{\boldsymbol{\Psi}}{\nu - p - 1} \text{ for } \nu > p + 1.$$

Hence, in the Random Covariance Model (RCM) of (2.1), $\boldsymbol{\Sigma}$ can be interpreted as a location-like parameter as it is the expected covariance matrix in each study. The parameter ν inversely controls the inter-study variation and can as such be considered an inter-study homogeneity parameter of the covariance structure. A large ν corresponds to high study homogeneity and vice versa for small ν . This can further be seen as $\boldsymbol{\Sigma}_i$ concentrates around $\boldsymbol{\Sigma}$ for $\nu \rightarrow \infty$ which corresponds to a vanishing inter-study variation for increasing ν . This fact is seen directly from variance and covariance expressions for the inverse Wishart (see (F.2) and (F.3)) where the 4th order denominator grows much faster than the 1st order nominator as polynomials in ν and causing the variance to vanish for $\nu \rightarrow \infty$. Thus, the true underlying covariance matrix $\boldsymbol{\Sigma}$ and the homogeneity parameter ν are the effects of interest to be estimated.

2.1. *The likelihood function.* Suppose $\mathbf{x}_{i1}, \dots, \mathbf{x}_{in_i}$ are n_i i.i.d. observations from $i = 1, \dots, k$ independent studies from the model given in (2.1). Let $\mathbf{X}_i = (\mathbf{x}_{i1}, \dots, \mathbf{x}_{in_i})^\top$ be the $n_i \times p$ matrix of observations for the i 'th study where rows correspond to samples and columns to variables. By the independence assumptions, the log-likelihood for $\boldsymbol{\Psi}$ and ν is given by

$$\begin{aligned} \ell(\boldsymbol{\Psi}, \nu | \mathbf{X}_1, \dots, \mathbf{X}_k) &= \log f(\mathbf{X}_1, \dots, \mathbf{X}_k | \boldsymbol{\Psi}, \nu) \\ &= \log \int f(\mathbf{X}_1, \dots, \mathbf{X}_k | \boldsymbol{\Sigma}_1, \dots, \boldsymbol{\Sigma}_k, \boldsymbol{\Psi}, \nu) f(\boldsymbol{\Sigma}_1, \dots, \boldsymbol{\Sigma}_k | \boldsymbol{\Psi}, \nu) d\boldsymbol{\Sigma}_1 \cdots d\boldsymbol{\Sigma}_k \\ &= \log \prod_{i=1}^k \int f(\mathbf{X}_i | \boldsymbol{\Sigma}_i) f(\boldsymbol{\Sigma}_i | \boldsymbol{\Psi}, \nu) d\boldsymbol{\Sigma}_i. \end{aligned}$$

Throughout, we use the generic notation $f(\cdot|\cdot)$ and $f(\cdot)$ for the conditional and unconditional pdf of random variables, respectively. Since the inverse Wishart distribution is conjugate to the multivariate Gaussian distribution, the integral—of which the integrand forms a Gaussian-inverse-Wishart distribution—can be evaluated. Hence $\boldsymbol{\Sigma}_i$ can be marginalized out, cf. (B.4) in Appendix B, and we arrive at the following expression for the log-likelihood function,

$$\begin{aligned}
 \ell(\boldsymbol{\Psi}, \nu | \mathbf{X}_1, \dots, \mathbf{X}_k) &= \log \prod_{i=1}^k \frac{|\boldsymbol{\Psi}|^{\frac{\nu}{2}} \Gamma_p\left(\frac{\nu+n_i}{2}\right)}{\pi^{\frac{n_i p}{2}} |\boldsymbol{\Psi} + \mathbf{X}_i^\top \mathbf{X}_i|^{\frac{\nu+n_i}{2}} \Gamma_p\left(\frac{\nu}{2}\right)} \\
 (2.3) \quad &= \sum_{i=1}^k \left[\frac{\nu}{2} \log |\boldsymbol{\Psi}| - \frac{\nu+n_i}{2} \log |\boldsymbol{\Psi} + \mathbf{X}_i^\top \mathbf{X}_i| + \log \frac{\Gamma_p\left(\frac{\nu+n_i}{2}\right)}{\Gamma_p\left(\frac{\nu}{2}\right)} \right],
 \end{aligned}$$

up to an additive constant where Γ_p is the multivariate generalization of the gamma function Γ , see (B.3). The scatter matrix $\mathbf{S}_i = \mathbf{X}_i^\top \mathbf{X}_i$ and study sample size n_i are sufficient statistics for each study. Note that \mathbf{S}_i is conditionally Wishart distributed, $\mathbf{S}_i | \boldsymbol{\Sigma}_i \sim \mathcal{W}(\boldsymbol{\Sigma}_i, n_i)$, by construction.

As stated in the following two propositions, the likelihood is not log-concave in general. However, it is log-concave as a function of ν . All proofs have been deferred to Appendix C.

PROPOSITION 1 (Non-concavity in $\boldsymbol{\Psi}$). *For a fixed ν , the log-likelihood function (2.3) is not concave in $\boldsymbol{\Psi}$.*

PROPOSITION 2 (Concavity in ν). *For a fixed positive definite $\boldsymbol{\Psi}$, the log-likelihood function (2.3) is concave in ν .*

While the likelihood function is not concave in $\boldsymbol{\Psi}$ we are able to show the existence and uniqueness of a global maximum in $\boldsymbol{\Psi}$.

PROPOSITION 3 (Existence and uniqueness). *The log-likelihood (2.3) has a unique maximum in $\boldsymbol{\Psi}$ for fixed ν and $n_\bullet = \sum_{a=1}^k n_a \geq p$.*

In the following section estimators of the parameters are derived using moments and the EM algorithm assuming ν to be fixed.

2.2. Moment estimator. The pooled empirical covariance matrix can be viewed as a moment estimator of $\boldsymbol{\Sigma}$. By the model assumptions, the first

and second moment of the j 'th observation in the i 'th study, \mathbf{x}_{ij} , is given by $\mathbb{E}[\mathbf{x}_{ij}] = \mathbf{0}_p$ and

$$\mathbb{E}[\mathbf{x}_{ij}\mathbf{x}_{ij}^\top] = \mathbb{E}\left[\mathbb{E}[\mathbf{x}_{ij}\mathbf{x}_{ij}^\top|\boldsymbol{\Sigma}_i]\right] = \mathbb{E}[\boldsymbol{\Sigma}_i] = \frac{\boldsymbol{\Psi}}{\nu - p - 1} = \boldsymbol{\Sigma}.$$

for all $j = 1, \dots, n_i$ and $i = 1, \dots, k$. This suggests the estimators

$$(2.4) \quad \hat{\boldsymbol{\Psi}}_{\text{pool}} = (\nu - p - 1) \frac{\sum_{i=1}^k \mathbf{S}_i}{\sum_{i=1}^k n_i} \quad \text{and} \quad \hat{\boldsymbol{\Sigma}}_{\text{pool}} = \frac{\sum_{i=1}^k \mathbf{S}_i}{\sum_{i=1}^k n_i}, \quad \nu > p + 1$$

where the latter is obtained by plugging $\hat{\boldsymbol{\Psi}}_{\text{pool}}$ into (2.2). This is the well-known pooled empirical covariance matrix.

2.3. Maximization using the EM algorithm. Here the updating scheme of the expectation-maximization (EM) algorithm (Dempster, Laird and Rubin, 1977) for fixed ν is derived. We now compute the expectation step of the EM-algorithm.

From (2.1) we have that,

$$\begin{aligned} \boldsymbol{\Sigma}_i &\sim \mathcal{W}_p^{-1}(\boldsymbol{\Psi}, \nu), \\ \mathbf{S}_i | \boldsymbol{\Sigma}_i &\sim \mathcal{W}_p(\boldsymbol{\Sigma}_i, n_i) \quad \text{for } i = 1, \dots, k. \end{aligned}$$

Let $\boldsymbol{\Delta}_i = \boldsymbol{\Sigma}_i^{-1}$ be the precision matrix and let $\boldsymbol{\Theta} = \boldsymbol{\Psi}^{-1}$, then we equivalently have that

$$(2.5) \quad \begin{aligned} \boldsymbol{\Delta}_i &\sim \mathcal{W}_p(\boldsymbol{\Theta}, \nu), \\ \mathbf{S}_i | \boldsymbol{\Delta}_i &\sim \mathcal{W}_p(\boldsymbol{\Delta}_i^{-1}, n_i). \end{aligned}$$

From the conjugacy of the inverse Wishart and the Wishart distribution, the posterior distribution of the precision matrix is

$$\boldsymbol{\Delta}_i | \mathbf{S}_i \sim \mathcal{W}_p\left((\boldsymbol{\Theta}^{-1} + \mathbf{S}_i)^{-1}, n_i + \nu\right).$$

Hence, by the expectation of the Wishart distribution,

$$\mathbb{E}[\boldsymbol{\Delta}_i | \mathbf{S}_i] = (n_i + \nu)(\boldsymbol{\Theta}^{-1} + \mathbf{S}_i)^{-1}.$$

The maximization step, in which the log-likelihood $\ell(\boldsymbol{\Theta} | \boldsymbol{\Delta}_1, \dots, \boldsymbol{\Delta}_k)$ is maximized, yields the estimate $\hat{\boldsymbol{\Theta}} = \frac{1}{k\nu} \sum_{i=1}^k \boldsymbol{\Delta}_i$, which is the mean of the scaled precision matrices $\frac{1}{\nu} \boldsymbol{\Delta}_i$ (derived in Appendix D). Let $\hat{\boldsymbol{\Theta}}_{(t)}$ be the current estimate of $\boldsymbol{\Theta}$. This yields the updating scheme

$$(2.6) \quad \hat{\boldsymbol{\Theta}}_{(t+1)} = \frac{1}{k\nu} \sum_{i=1}^k (n_i + \nu) \left(\hat{\boldsymbol{\Theta}}_{(t)}^{-1} + \mathbf{S}_i \right)^{-1}$$

Algorithm 1 RCM coordinate ascent estimation procedure

```

1: Input:
2: Sufficient data:  $(\mathbf{S}_1, n_1), \dots, (\mathbf{S}_k, n_k)$ 
3: Initial parameters:  $\hat{\Psi}_{(0)}, \hat{\nu}_{(0)}$ 
4: Convergence criterion:  $\varepsilon > 0$ 
5: Output:
6: Parameter estimates:  $\hat{\Psi}, \hat{\nu}$ 
7: procedure FITRCM( $\mathbf{S}_1, \dots, \mathbf{S}_k, n_1, \dots, n_k, \hat{\Psi}_{(0)}, \hat{\nu}_{(0)}, \varepsilon$ )
8:   Initialize:  $l_{(0)} \leftarrow \ell(\hat{\Psi}_{(0)}, \hat{\nu}_{(0)})$ 
9:   for  $t = 1, 2, 3, \dots$  do
10:     $\hat{\Psi}_{(t)} \leftarrow U(\hat{\Psi}_{(t-1)}, \hat{\nu}_{(t-1)})$ 
11:     $\hat{\nu}_{(t)} \leftarrow \arg \max_{\nu} \ell(\hat{\Psi}_{(t)}, \nu)$ 
12:     $l_{(t)} \leftarrow \ell(\hat{\Psi}_{(t)}, \hat{\nu}_{(t)})$ 
13:    if  $l_{(t)} - l_{(t-1)} < \varepsilon$  then
14:      return  $(\hat{\Psi}_{(t)}, \nu_{(t)})$ 
15:    end if
16:  end for
17: end procedure

```

for $\Theta_{(t)}$. We denote the inverse of the estimate obtained by repeated iteration of (2.6) by $\hat{\Psi}_{\text{EM}}$. The EM algorithm can be sensitive to starting values. Hence, starting the algorithm in different starting values can help assessing if a global maximum has been reached.

An approximate maximum likelihood estimator using a first order approximation is also possible (derived in Appendix E).

2.4. Estimation procedure. We propose a procedure alternating between estimating ν and Ψ while keeping the other fixed. Given parameters $\hat{\nu}_{(t)}$ and $\hat{\Psi}_{(t)}$ at iteration t , we estimate $\hat{\Psi}_{(t+1)}$ using fixed $\hat{\nu}_{(t)}$. Subsequently, we find $\hat{\nu}_{(t+1)}$ by a standard one-dimensional numerical optimization procedure using the fixed $\hat{\Psi}_{(t+1)}$. This coordinate ascent approach is repeated until convergence as described in Algorithm 1. The update function U in the algorithm is defined by the derived estimators. That is, equations (2.4), (2.6), or (E.2) define U as the pooled, EM, or approximate MLE estimates, respectively.

The procedure using the EM step utilizes the results about the RCM log-likelihood and thus provides a guarantee of convergence along with the advantage of a very simple implementation. Both the EM step and the ν update will always yield an increase in the likelihood. The disadvantage is that the identified stationary point might be a local maximum or saddle-point when considering the log-likelihood function jointly in (Ψ, ν) . Intuitively, the

latter possibility happens with zero probability, but it cannot be excluded that the maximum found is not global.

Variations on the convergence criterion can also be considered, such as (a) using the difference in successive parameter estimates, or (b) using relative rather than absolute differences.

2.5. Interpretation and inference.

Intra-study correlation coefficient. The heterogeneity parameter ν has no straightforward interpretation partly because the values of ν which corresponds to a large study heterogeneity is dependent on the dimension p . We therefore introduce a descriptive statistic analogous to the intra-study correlation coefficient (ICC) (Shrout and Fleiss, 1979) well known from ordinary meta-analysis. For the RCM this follows from the definition of the ICC which is defined to be the ratio of the between-study variation $\text{Var}(\Sigma_{ij})$ and the total variation $\text{Var}(S_{ij})$ of any single pair of variables. In Appendix F it is shown that the ICC is given by:

$$(2.7) \quad \text{ICC}(\nu) = \frac{1}{\nu - p}.$$

The ICC might in this sense be utilized in better quantifying the reproducibility of the covariance across studies. A straight-forward plug-in estimator $\widehat{\text{ICC}}(\hat{\nu})$ of the ICC of some gene-gene interaction is then $\text{ICC}(\hat{\nu})$.

Though $\nu > p + 3$ is required for the variances to exist, it is clear that $\text{ICC}(\nu) \rightarrow 1$ for $\nu \rightarrow (p + 1)^+$ and $\text{ICC}(\nu) \rightarrow 0$ for $\nu \rightarrow \infty$ as should be expected.

Test for no study heterogeneity. By the RCM ν parameterizes an inter-study variance where the size of ν corresponds to the homogeneity between the studies. A large ν yields high study homogeneity while a small ν yields low homogeneity. Thus, it might be of interest to test if the estimated homogeneity $\hat{\nu}$ is extreme under the null-hypothesis of no heterogeneity (i.e. infinite homogeneity). I.e. a test for the hypothesis $H_0 : \nu = \infty$ which is equivalent to

$$H_0 : \Sigma_1 = \dots = \Sigma_k = \Sigma.$$

The two are equivalent since sampling the covariance matrix from the inverse Wishart distribution becomes deterministic for $\nu = \infty$. Therefore, testing this hypothesis can also be interpreted as testing whether the data is adequately explained when leaving out the hierarchical structure.

The distribution of $\hat{\nu}$ under the null hypothesis is not tractable. However, in practice under H_0 or when ν is extremely large the estimated $\hat{\nu}_{\text{obs}}$ will be finite as the intra-study variance dominates the total variance. We note that the null distribution of $\hat{\nu}$ does not depend on Σ . We propose approximating the distribution of $\hat{\nu}$ under H_0 by resampling. To do this, the model is simply fitted a large number of times N on datasets re-sampled under H_0 mimicked by permuted study labels to get $\hat{\nu}_0^{(1)}, \dots, \hat{\nu}_0^{(N)}$. As *small* values of $\hat{\nu}$ are critical for H_0 approximate acceptance regions can be constructed from $\hat{\nu}_0^{(j)}, j = 1, \dots, N$. Likewise, an approximation of the p value testing H_0 can be obtained by

$$(2.8) \quad P = \frac{1}{N+1} \left(1 + \sum_{j=1}^N \mathbb{1}[\hat{\nu}_0^{(j)} < \hat{\nu}_{\text{obs}}] \right),$$

where $\mathbb{1}[\cdot]$ is the indicator function. The addition of one to both nominator and denominator adds a positive bias to the approximate p-value and is considered minimally needed according to [Phipson and Smyth \(2010\)](#). This is approximately the fraction of $\hat{\nu}_0^{(j)}$'s smaller than $\hat{\nu}_{\text{obs}}$.

2.6. Implementation and availability. Algorithm 1 and the different estimators are implemented in the statistical programming language R ([R Core Team, 2012](#)) with core functions in C++ using packages Rcpp and RcppArmadillo ([Eddelbuettel and François, 2011](#); [François, Eddelbuettel and Bates, 2012](#)). They are incorporated in the open-source R-package `correlateR` freely available for forking and editing ([Bilgrau, 2014](#)). We refer to the information here for further details and installation instructions. This document was prepared with `knitr` ([Xie, 2013](#)) and LaTeX. To reproduce this document see <http://github.com/AEBilgrau/RCM>.

3. Simulation experiments.

3.1. Evaluation of Network Estimation. To assess the estimation procedures ability to estimate Σ we generated data from the hierarchical model (2.1) in two different scenarios. In the first scenario we define a simple block matrix of dimension $p = 40$ with four blocks of size 10. Each block has an internal pairwise correlation of 0.5, blocks 1 and 2 and 3 and 4 have a correlation of 0.3 between all pairs, and the remaining correlations are set at 0.1. In the second scenario we select the top 100 genes, ranked by variance, from the IDRC dataset (see Table 2) and used the scatter matrix of these genes, scaled as a correlation matrix, as the Σ matrix for simulation. For both scenarios we performed agglomerative hierarchical clustering using

Ward-linkage and 1 minus the absolute correlation as a distance measure. Heatmaps with associated hierarchical clustering of both Σ matrices are shown in Supplementary Figure A.1.

For both scenarios we simulate data with $k = 3$ and a range of values for n_i and ν . Each simulation was repeated 100 times, and the correlation matrix was estimated using the EM, MLE, and Pool approaches as outlined in Section 2. The similarity of the estimated and true Σ matrices and associated networks were evaluated using respectively the Kullback-Leibler divergence (Mattiussi et al., 2011) and the cophenetic correlation (Sokal and Rohlf, 1962). The cophenetic correlation is defined as the correlation of cophenetic distances of all pairwise distances in a tree, where the cophenetic distance is the height of the lowest point on the tree where two points merge. Results from the first scenario (EM and Pool method in Table 1, full results in Supplementary Table A.1) show that for heterogeneous data ($\nu = 50, 100$) and $n_i \geq p$ the EM estimator outperforms the Pool and MLE estimators using both measures. Examples of tanglegrams comparing networks estimated with the EM and Pool method and the true Σ matrix are shown in Supplementary Figure A.2. Tanglegrams were constructed using the R-package `dendextend` (Galili, 2015). Increasing the ν parameter, thereby making the data more homogeneous across groups diminishes the advantage of the EM estimator. Similar results were found in the second scenario using a Σ matrix based on the IDRC dataset (Table A.2). Results furthermore showed that the estimates in terms of cophenetic correlation for the MLE and Pool approaches are nearly identical. We expect this to be caused by the fact that the MLE method is initialized with the Pool estimates and stops after few iterations; presumably a better estimate cannot be found in these simple scenarios.

3.2. Computation time for the RCM model. Next we tested the performance of the different methods in terms of computation time. Figure 1 shows computation times of the methods with varying values of the dimension of the data, and demonstrates that the increased performance of the EM method comes at an extra cost in computation time.

3.3. Evaluation of the hypothesis testing. Finally we investigate the performance of the P-value for the hypothesis test suggested in (2.8). To do this, we simulate from the hierarchical model with $k = 3$ and a range of different values for p , ν , and n_i . For these simulations we used a Ψ matrix with a diagonal of ones and 0.5 for off-diagonal values. Simulations were done 100 times for each scenario, and 500 permutations were done for each simulation. Results summarized as boxplots of the P-values obtained in the

TABLE 1

Mean cophenetic correlation and Kullback-Leibler divergence with 95% confidence, for estimated vs true network for different values of ν and n_i using the EM or Pool method

n_i	ν	Cophenetic Correlation		Kullback-Leibler divergence	
		EM	Pool	EM	Pool
20	50	0.19 (0.17;0.21)	0.2 (0.18;0.22)	240.37 (232.79;247.94)	227.33 (220.13;234.52)
30	50	0.26 (0.23;0.28)	0.25 (0.23;0.28)	126.61 (123.81;129.41)	121.81 (119.1;124.51)
50	50	0.6 (0.56;0.64)	0.43 (0.39;0.46)	75.62 (73.5;77.74)	73.62 (71.54;75.69)
100	50	0.88 (0.85;0.9)	0.7 (0.67;0.74)	33.04 (32.56;33.52)	30.9 (30.44;31.36)
500	50	0.99 (0.98;0.99)	0.91 (0.89;0.93)	23.64 (23.41;23.88)	21.31 (21.1;21.53)
1000	50	0.99 (0.99;0.99)	0.9 (0.88;0.92)	22.86 (22.59;23.14)	20.53 (20.28;20.78)
20	100	0.35 (0.32;0.38)	0.35 (0.32;0.37)	76.69 (74.05;79.33)	72.36 (69.85;74.86)
30	100	0.4 (0.37;0.42)	0.39 (0.37;0.42)	34.51 (33.76;35.26)	33.14 (32.42;33.87)
50	100	0.72 (0.68;0.75)	0.69 (0.66;0.72)	27.92 (27.2;28.65)	27.26 (26.55;27.97)
100	100	0.97 (0.96;0.98)	0.96 (0.95;0.97)	8.02 (7.88;8.16)	7.85 (7.71;7.98)
500	100	1 (0.99;1)	1 (1;1)	3.34 (3.31;3.38)	3.18 (3.15;3.21)
1000	100	1 (1;1)	1 (1;1)	2.95 (2.92;2.98)	2.79 (2.77;2.82)
20	1000	0.51 (0.48;0.54)	0.51 (0.48;0.54)	52.66 (51.04;54.29)	49.61 (48.07;51.16)
30	1000	0.61 (0.58;0.64)	0.61 (0.58;0.64)	22.5 (22.05;22.95)	21.59 (21.16;22.02)
50	1000	0.81 (0.78;0.84)	0.81 (0.78;0.84)	20.49 (19.91;21.08)	20.02 (19.44;20.59)
100	1000	0.99 (0.98;0.99)	0.99 (0.99;0.99)	4.47 (4.36;4.58)	4.42 (4.31;4.52)
500	1000	1 (1;1)	1 (1;1)	0.71 (0.7;0.72)	0.71 (0.7;0.72)
1000	1000	1 (1;1)	1 (1;1)	0.41 (0.41;0.42)	0.41 (0.4;0.42)
20	10000	0.53 (0.5;0.55)	0.52 (0.5;0.55)	53.15 (51.26;55.04)	50.07 (48.28;51.86)
30	10000	0.65 (0.61;0.68)	0.64 (0.61;0.68)	21.91 (21.46;22.35)	21.01 (20.59;21.44)
50	10000	0.83 (0.8;0.85)	0.82 (0.79;0.85)	19.88 (19.29;20.48)	19.42 (18.84;20.01)
100	10000	0.99 (0.99;1)	0.99 (0.99;1)	4.19 (4.11;4.27)	4.14 (4.06;4.22)
500	10000	1 (1;1)	1 (1;1)	0.59 (0.58;0.6)	0.59 (0.58;0.6)
1000	10000	1 (1;1)	1 (1;1)	0.28 (0.27;0.28)	0.28 (0.27;0.28)

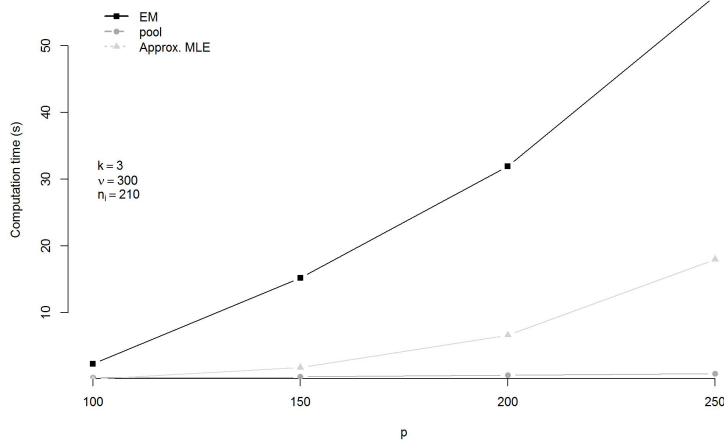


Fig 1: The mean computation time of 10 fits with varying dimension p .

100 simulations for each scenario are shown in Supplementary Figure A.3. We find that for heterogenous data (e.g. $p = 20, \nu = 30$) the null-hypothesis is clearly rejected if $n_i > p$. When increasing ν thus making the groups more similar, more observations are needed to reject the null hypothesis, while for identical groups, i.e. $\nu = \infty$, the null-hypothesis is generally not rejected. The P-values obtained from the permutation test thus performs as intended.

4. DLBCL meta-analysis. Diffuse large B-cell lymphoma (DLBCL) is an aggressive cancer subtype accounting for 30% – 58% of non-Hodgkin’s lymphomas (NHL) which constitutes about 90% of all lymphomas ([International Lymphoma Study Group, 1997](#)).

4.1. Data and preprocessing. A large amount of DLBCL gene expression datasets are now available online at the NCBI (National Center for Biotechnology Information) Gene Expression Omnibus (GEO) website. Ten large-scale DLBCL gene expression studies were downloaded and preprocessed using custom brainarray chip definition files (CDF) ([Dai et al., 2005](#)) and RMA-normalized using the R-package `affy` ([Gautier et al., 2004](#)). The corresponding GEO-accession numbers and microarray platforms used are seen in Table 2. The downloaded data yield a total of 2046 samples with study sizes in the range 78-469. The summarization using brainarray CDFs to Ensembl gene identifiers facilitates cross-platform integration.

After RMA normalization and summarization, the data were brought to a common scale by quantile normalizing all data to the common cumulative distribution function of all arrays. Lastly, the datasets were reduced to 11573 common genes represented in all studies and array platforms. Figure A.4 shows a plot of the first and second principal components of the combined dataset. We see a clear split on the first principal component, indicating a possible batch effect and heterogeneous data, and thus a situation where the EM estimator might offer an advantage compared to the simpler Pool approach.

4.2. Analysis. For each dataset the scatter matrix \mathbf{S}_i of the top 300 most variable genes (as measured by the pooled variance across all studies) was computed as the sufficient statistics along with the number of samples.

The parameters of the RCM were estimated using the EM algorithm and yielded the 300×300 matrix $\hat{\Psi}$, $\hat{\nu} = 773.16$, and $\text{ICC} = 0.0021$. The RCM was fitted using three different initial sets of parameters which all converged to the same parameter estimates. Log-likelihood traces, iterations used, and computation times are seen in Figure 2. From the parameter

TABLE 2

Overview of studies used with GEO accession number from the NCBI Gene expression omnibus website, the relevant reference, array types used in the study, and number of samples and features on the used array.

	GEO no.	Name	Reference	Used arrays	n
1	GSE56315	CHEPRETRO	Dybkær et al. (2015)	hgu133plus2	89
2	GSE19246	BCCA	Williams et al. (2010)	hgu133plus2	177
3	GSE12195	CUICG	Compagno et al. (2009)	hgu133plus2	136
4	GSE22895	HMRC	Jima et al. (2010)	hugene10st	101
5	GSE31312	IDRC	Visco et al. (2012)	hgu133plus2	469
6	GSE10846	LLMPP R-CHOP	Lenz et al. (2008)	hgu133plus2	181
7	GSE10846	LLMPP CHOP	Lenz et al. (2008)	hgu133plus2	233
8	GSE34171	MDFCI	Monti et al. (2012)	hgu133plus2, snp6	90
9	GSE34171	MDFCI	Monti et al. (2012)	hgu133a, hgu133b	78
10	GSE22470	MMML	Salaverria et al. (2011)	hgu133a	271
11	GSE4475	UBCBF	Hummel et al. (2006)	hgu133a	221

estimate, the common expected covariance $\hat{\Sigma} = (\hat{\nu} - p - 1)^{-1} \hat{\Psi}$ was computed and subsequently scaled to the corresponding correlation matrix \hat{R} .

Despite the low ICC value the permutation test yielded a P-value for the null hypothesis of study homogeneity of 0.002, clearly rejecting it. This means a significant difference has been detected between the estimated covariance structures across studies. This low ICC might suggest selecting the most variable genes bias the ICC towards inter-study homogeneity of covariances. To further investigate the low ICC value we randomly sampled 300 genes and estimated the ν parameter 100 times. This gave a value of ν ranging from 382.69 to 395.18 with a mean of 388.87, corresponding to an ICC ranging from 0.0105 to 0.0121 with a mean of 0.0113; histograms are shown in Supplementary Figure A.7. This indicates a bias towards more homogeneity for the high variance selected genes.

For simplicity we employed a standard network analysis to the estimated common correlation matrix \hat{R} across all studies. To identify clusters with high internal correlation, we used agglomerative hierarchical clustering with Ward-linkage and distance measure defined as 1 minus the absolute value of the correlation. The dendrogram was arbitrarily pruned at a height which produced 5 modules. The Modules are given different colors. Figure 3 shows the heatmap, associated network modules and suggested function.

We checked if the identified modules were prognostic for overall survival (OS) in the CHOP and R-CHOP-treated cohort datasets of GSE10846. To

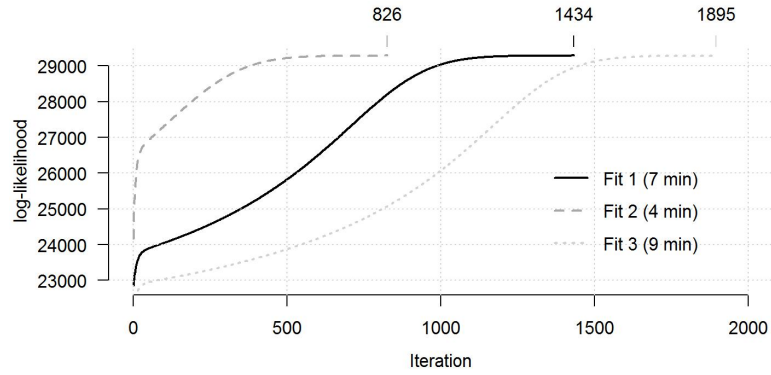


Fig 2: The trace of the log-likelihood for three different starting values of Ψ and ν using the EM algorithm and computational times in minutes. The number of iterations used for each fit is shown above.

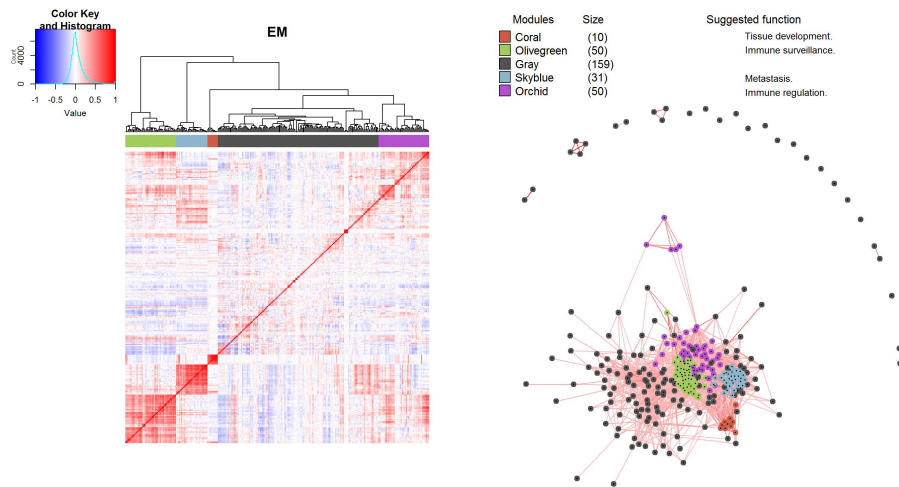


Fig 3: Heatmap and correlation network for the estimated correlation matrices of the top 300 genes for the DLBCL data using the EM method. The network is cut at a height producing 5 clusters

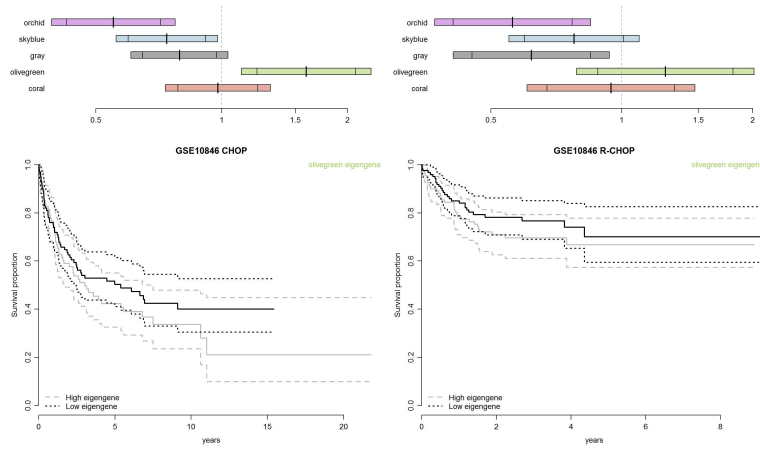


Fig 4: The top row shows 95% and 99% CI for the hazard ratio for each eigengene in the multiple Cox proportional hazards model containing all eigengenes in the CHOP and R-CHOP dataset. The bottom row shows Kaplan-Meier estimates (and 95% CI) for the overall survival for patients stratified by the dichotomized olivegreen eigengene.

do this, the eigengene (Horvath, 2011) for each module was computed. The module eigengene is the first principal component of the expression matrix of the module which thus can be represented by a linear combination of the module genes. We also report the amount of variation the eigengene represents by calculating the explained variation of the first principal component. Multiple Cox proportional hazards model for OS was fitted with the module eigengenes as covariates. For the prognostically interesting and tightly clustered olivegreen module, the Kaplan-Meier estimates were computed for groups arising when dichotomizing the values of the corresponding eigengene as above or below the median value. These results are shown in Figure 4. The proportion of variance explained by the eigengene in the CHOP and R-CHOP datasets for respectively the Coral, Olivegreen, Gray, Skyblue and Orchid modules were 0.72, 0.6, 0.11, 0.7, 0.31, and 0.77, 0.55, 0.11, 0.7, 0.31.

Next, the modules were screened for biological relevance using GO (Gene Ontology) Biological Process, Molecular Function, and Cellular Component as well as REACTOME and KEGG pathway enrichment analysis. This was done using the g:profiler web server (Reimand et al., 2016) via the accompanying R-package gProfileR (Reimand, Kolde and Arak, 2016). Since we pre-selected the top 300 genes by variance, the enrichment analysis was done using only these as the background genes. Top genes for each module,

Gray n = 159	Olivegreen n = 50	Orchid n = 50	Skyblue n = 31	Coral n = 10
MYBL1	FCER1G	CD2	COL5A2	KRT6A
BATF	C1QB	CD3D	COL1A2	SPRR1A
STAP1	C1QA	GIMAP4	COL3A1	SPRR1B
CYB5R2	GBP1	PTGDS	THBS2	KRT13
TNFRSF13B	RARRES3	CCL19	COL6A3	SPRR3
CD44	IDO1	CLU	COL1A1	S100A2
MARCKSL1	CD14	ADAMDEC1	COL5A1	KRT14
LRMP	LILRB2	TRBC2	VCAN	DSP
HCK	SERPING1	ITM2A	FAP	KRT5
MME	PSTPIP2	LGALS2	MMP2	
LMO2	GZMA	ITK	SULF1	
VPREB3	CCL8	PLA2G2D	MXRA5	
BCL2A1	IFNG	IL7R	DCN	
BLNK	GBP2	PLA2G7	LUM	
HLA-DOB	CXCL10	ENPP2	SPARC	
RRAS2	SLAMF7	IL18	POSTN	
STAG3	FGL2	CHI3L1	COL15A1	
BACH2	CD163	TFEC	TMEM45A	
CCND2	CXCL11	CXCL13	COL11A1	
PDGFD	GZMH	CCL21	CTSK	
NCF2	ALDH1A1	CSTA	EMP1	
SPINK2	CXCL9	MMP9	AEBP1	
MNDA	GZMK	LYZ	TGFBI	
MS4A1	GZMB	HSD11B1	GJA1	
CD22	KCNJ2	APOC1	PLS3	
OSBP10	CPVL	CXCL14	TIMP1	
GPR137B	IGSF6	C3	ANXA1	
GRHR	LGMN	MAL	TNFAIP6	
SORL1	MT2A	CYP27B1	SPP1	
IGF2BP3	MT1G	LAMP3		
SYBU	CD8A	CHIT1		
TCL1A	MS4A4A	PLAC8		
ZNF804A	CRTAM	SELL		
SLC12A8	S100A9	KLRB1		
CTGF	MARCO	CD69		
FCRL2	S100A8	ROBO1		
DUSP5	MT1M	ORM1		
CCR10	GPX3	S1PR1		
ALOX5AP	GNLY	CCR7		
RGCC	MT1E	GPR183		

TABLE 3

The identified modules, their sizes, and member genes. The genes are sorted decreasingly by their intra-module connectivity (sum of the incident edge weights). Only the top 40 genes are shown.

ranked by connectivity, are shown in Table 3, while results of the enrichment analysis for each of the modules are shown in Supplementary Table A.3. Inspection of the enrichment analysis and most connected genes allowed us to hypothesize that the coral module is involved in "tissue development" (strong association with GO:0009888 tissue development), the Skyblue module is involved in "metastasis" (strong association with GO:0009611-response to wounding and GO:00442060-wound healing, (Arnold et al., 2015)), the orchid module involved in "immune regulation" (strong association with GO:0002376-immune system process), and the olivegreen module involved in "immune surveillance" (strong association with GO:0006952-defense response and GO:0045087-innate immune response).

From the gene enrichment and survival analysis the olivegreen module appeared particularly interesting, as we notice a strong involvement of immune

response and an association between high value of the eigengene expression and poor survival, which eventually could make these patients candidates for experimental immunotherapies. Several of the genes, e.g. S100A8, S100A9, CD14, and CD163 with the highest connectivity in this module have been associated to immunotherapy (Fulmer, 2008; Cheng et al., 2008; Stroncek et al., 2017). As prominent examples S100A8 (MRP8; calgranulin A) and the gene S100A9 (MRP14; calgranulin B) appear in the list. This is interesting as compelling research has shown that the S100 family of calcium-binding proteins maintain immunosuppressive myeloid-derived suppressor (MDS) cells at the tumor site (Fulmer, 2008). Notably, in mice injected with lymphoma cells, knockout of S100A9 resulted in greater tumor infiltration of T-cells and less accumulation of MDS cells than that seen in wild-type mice (Cheng et al., 2008). The knockout mice had higher rates of tumor rejection and lower tumor size than their wild-type littermates. This result indicates that knockdown of these proteins may improve the outcome of immunotherapy strategies in patients with values of the eigengene of the olivegreen module.

Finally, we compared the network analyses based on the covariance matrix obtained by the EM to that obtained by the Pool methods. The upper row of Supplementary Figure A.5 shows the heatmap and associated network modules for the Pool method, when the dendrogram is cut at 5 modules, Supplementary Figure A.6 shows plots for the survival analysis, and top genes and gene enrichments are given in Supplementary Tables A.4 and A.5. For the Pool method, we chose for each module the same color as the module of the EM based clustering with most overlapping genes. In the lower row of Figure A.5 a tanglegram was constructed and the cophenetic correlation was calculated. We noticed generally a great overlap between the modules, but a low cophenetic correlation. With background in the simulation we anticipate the Pool method has lower efficiency than the EM method.

The olivegreen and coral modules seem to be so tightly regulated that they manifest themselves for both methods, which is also seen in the enrichment analyses. However, the size of the skyblue module is increased for the pool method by acquiring genes from the grey module identified by the EM method, but the overall enrichment is not changed. For the orchid module, we notice a number of genes ending up in the grey module for the pool method. This has the consequence that the immune regulation fingerprint disappears using the pool method. Moreover, if we look at the less correlated intramodular connections the noise plays a larger role leading to a less clear separation between the modules for the Pool method. This can have potential biological implications, when regulating hub genes resulting in intra module cascades of reactions.

5. Discussion. The RCM for meta-analysis of covariance structures was shown to be superior to simple pooling as suggested previously in the literature. The estimated covariance matrix was also capable of providing a dissimilarity measure, which was able to pinpoint alternative biologically meaningful gene correlation networks in DLBCL, which can be used to formulate new hypothesis about the role of immune therapy in DLBCL.

However, the proposed testing is computationally demanding and only feasible when p is sufficiently small. This could e.g. be overcome by improved and faster fitting procedures or by deriving the distribution of $\hat{\nu}$ under the null hypothesis. Yet the latter is seemingly intractable as $\hat{\nu}$ is a very complex function of the data. The fact that the null-hypothesis lies on the edge of the parameter space also seems to constrain the feasibility of deriving such a distribution. One might question whether the added utility of the ν parameter provides sufficient relaxation of the covariance homogeneity. Therefore, the present work should be considered a first step in the direction of explicitly modelling the inter-study variation of covariance matrices. It is also worth noticing, that although the suggested method proved to be superior to simple pooling, it only works for small or moderate numbers of features p . This can partly be alleviated by combining multiple studies to yield a sufficiently large total sample size n_{\bullet} that allows for the estimation of large covariance matrices. Turning to using p -values seems tempting, but one should be aware, as with all hypothesis testing, that the exact threshold of ICC (or ν) needed to claim homogeneous studies is dependent on the sample size and the relevant effect size. In this respect the relevant effect size is unclear and will be problem dependent.

The moderate size of p is a severe drawback as many methods have been published concerning estimation of large covariance matrices by various regularization methods (Meinshausen and Bühlmann, 2006; Friedman, Hastie and Tibshirani, 2008; van Wieringen and Peeters, 2016). Therefore we believe this work could be further enriched by combining the method with regularized estimation. In the future such generalizations of the model to $p \gg n_{\bullet}$ is extremely interesting though out of scope for this article.

In conclusion the article demonstrates an advantageous model based way of conducting meta-analysis of covariance matrices - especially in a setting with moderate number of features compared to the dimension. One should also notice the method seems to provide a generally applicable framework making it usable in other settings where multiple features are measured and believed to share a common covariance matrix obscured by group dependent noise.

Acknowledgments. We thank Martin Raussen, Jon Johnsen, as well as Niels Richard Hansen for their assistance on some of the mathematical proofs. The helpful comments from Steffen Falgreen, Andreas S. Pedersen, and reviewers were also much appreciated. The technical assistance from Alexander Schmitz, Julie S. Bødker, Ann-Maria Jensen, Louise H. Madsen, and Helle Høholt is also greatly appreciated.

SUPPLEMENTARY MATERIAL

Supplement A: Appendices

(<http://imstat.org/aoas/>). Supplementary figures, tables and proofs available online.

Supplement B: Documents for reproducibility

(<http://github.com/AEBilgrau/RCM>). The documents and other needed files to perform the analyses to reproduce this article. See the README file herein.

References.

- AGNELLI, L., FORCATO, M., FERRARI, F., TUANA, G., TODOERTI, K., WALKER, B. A., MORGAN, G. J., LOMBARDI, L., BICCIATO, S. and NERI, A. (2011). The reconstruction of transcriptional networks reveals critical genes with implications for clinical outcome of multiple myeloma. *Clinical Cancer Research* **17** 7402–12.
- ARNOLD, K. M., OPDENAKER, L. M., FLYNN, D. and SIMS-MOURTADA, J. (2015). Wound healing and cancer stem cells: inflammation as a driver of treatment resistance in breast cancer. *Cancer Growth Metastasis* **8** 1–13.
- BILGRAU, A. E. (2014). correlateR: Fast, efficient, and robust partial correlations R package version 0.1, <http://github.com/AEBilgrau/correlateR>.
- BORENSTEIN, M., HEDGES, L. V., HIGGINS, J. P. and ROTHSTEIN, H. R. (2010). A basic introduction to fixed-effect and random-effects models for meta-analysis. *Res Synth Methods* **1** 97–111.
- CHENG, P., CORZO, C. A., LUETTEKE, N., YU, B., NAGARAJ, S., BUI, M. M., ORTIZ, M., NACKEN, W., SORG, C., VOGL, T. et al. (2008). Inhibition of dendritic cell differentiation and accumulation of myeloid-derived suppressor cells in cancer is regulated by S100A9 protein. *The Journal of experimental medicine* **205** 2235–2249.
- CHOI, J. K., YU, U., KIM, S. and YOO, O. J. (2003). Combining Multiple Microarray Studies and Modeling Interstudy Variation. *Bioinformatics* **19** i84–i90.
- CLARKE, C., MADDEN, S. F., DOOLAN, P., AHERNE, S. T., JOYCE, H., O'DRISCOLL, L., GALLAGHER, W. M., HENNESSY, B. T., MORIARTY, M., CROWN, J., KENNEDY, S. and CLYNES, M. (2013). Correlating transcriptional networks to breast cancer survival: a large-scale coexpression analysis. *Carcinogenesis* **34** 2300–2308.
- COMPAGNO, M., LIM, W. K., GRUNN, A., NANDULA, S. V., BRAHMACHARY, M., SHEN, Q., BERTONI, F., PONZONI, M., SCANDURRA, M., CALIFANO, A. et al. (2009). Mutations of multiple genes cause deregulation of NF- κ B in diffuse large B-cell lymphoma. *Nature* **459** 717–721.
- COOK, R. D. and FORZANI, L. (2011). On the Mean and Variance of the Generalized Inverse of a Singular Wishart Matrix. *Electronic Journal of Statistics* **5** 146–158.

- DAI, M., WANG, P., BOYD, A. D., KOSTOV, G., ATHEY, B., JONES, E. G., BUNNEY, W. E., MYERS, R. M., SPEED, T. P., AKIL, H., WATSON, S. J. and MENG, F. (2005). Evolving Gene/Transcript Definitions Significantly Alter the Interpretation of GeneChip Data. *Nucleic Acids Research* **33** e175.
- DEMPSTER, A. P., LAIRD, N. M. and RUBIN, D. B. (1977). Maximum Likelihood from Incomplete Data via the EM Algorithm. *Journal of the Royal Statistical Society, Series B (Statistical Methodology)* **39** 1–38.
- DERSIMONIAN, R. and LAIRD, N. (1986). Meta-analysis in Clinical Trials. *Controlled Clinical Trials* **7** 177–88.
- DYBKÆR, K., BØGSTED, M., FALGREEN, S., BØDKER, J. S., KJELDSSEN, M. K., SCHMITZ, A., BILGRAU, A. E., XU-MONETTE, Z. Y., LI, L., BERGKVIST, K. S., LAURSEN, M. B., RODRIGO-DOMINGO, M., MARQUES, S. C., RASMUSSEN, S. B., NYEGAARD, M., GAIHEDE, M., MØLLER, M. B., SAMWORTH, R. J., SHAH, R. D., JOHANSEN, P., EL-GALALY, T. C., YOUNG, K. H. and JOHNSEN, H. E. (2015). A Diffuse Large B-Cell Lymphoma Classification System That Associates Normal B-cell Subset Phenotypes with Prognosis. *Journal Of Clinical Oncology*, *In press*.
- EDDELBUEITTEL, D. and FRANÇOIS, R. (2011). Rcpp: Seamless R and C++ integration. *Journal of Statistical Software* **40**.
- FRANÇOIS, R., EDDELBUEITTEL, D. and BATES, D. (2012). RcppArmadillo: Rcpp Integration for Armadillo Templated Linear Algebra Library R package version 0.3.6.1.
- FRIEDMAN, J., HASTIE, T. and TIBSHIRANI, R. (2008). Sparse Inverse Covariance Estimation with the Graphical Lasso. *Biostatistics* **9** 432–41.
- FULMER, T. (2008). Suppressing the suppressors. **38**.
- GALILI, T. (2015). dendextend: An R package for visualizing, adjusting and comparing trees of hierarchical clustering. *Bioinformatics* **31** 3718–3720.
- GAUTIER, L., COPE, L., BOLSTAD, B. M. and IRIZARRY, R. A. (2004). affy—Analysis of Affymetrix GeneChip Data at the Probe Level. *Bioinformatics* **20** 307–315.
- INTERNATIONAL LYMPHOMA STUDY GROUP (1997). A Clinical Evaluation of the International Lymphoma Study Group Classification of Non-Hodgkin’s Lymphoma. *Blood* **89** 3909–3918.
- HORVATH, S. (2011). *Weighted Network Analysis: Applications in Genomics and Systems Biology*. Springer.
- HUMMEL, M., BENTINK, S., BERGER, H., KLAPPER, W., WESSENDORF, S., BARTH, T. F., BERND, H.-W., COGLIATTI, S. B., DIERLAMM, J., FELLER, A. C. et al. (2006). A biologic definition of Burkitt’s lymphoma from transcriptional and genomic profiling. *New England Journal of Medicine* **354** 2419–2430.
- IRIZARRY, R. A., HOBBS, B., COLLIN, F., BEAZER-BARCLAY, Y. D., ANTONELLIS, K. J., SCHERF, U. and SPEED, T. P. (2003). Exploration, normalization, and summaries of high density oligonucleotide array probe level data. *Biostatistics* **4** 249–264.
- JIMA, D. D., ZHANG, J., JACOBS, C., RICHARDS, K. L., DUNPHY, C. H., CHOI, W. W., AU, W. Y., SRIVASTAVA, G., CZADER, M. B., RIZZIERI, D. A. et al. (2010). Deep sequencing of the small RNA transcriptome of normal and malignant human B cells identifies hundreds of novel microRNAs. *Blood* **116** e118–e127.
- JOHNSON, W. E., LI, C. and RABINOVIC, A. (2007). Adjusting batch effects in microarray expression data using empirical Bayes methods. *Biostatistics* **8** 118–127.
- KHALIL, H. K. (2002). *Nonlinear Systems*. Prentice Hall.
- LEE, J., DOBBIN, K. K. and AHN, J. (2014). Covariance adjustment for batch effect in gene expression data. *Statistics in medicine* **33** 2681–2695.
- LENZ, G., WRIGHT, G. W., EMRE, N. T., KOHLHAMMER, H., DAVE, S. S., DAVIS, R. E., CARTY, S., LAM, L. T., SHAFFER, A., XIAO, W. et al. (2008). Molecular subtypes

- of diffuse large B-cell lymphoma arise by distinct genetic pathways. *Proceedings of the National Academy of Sciences* **105** 13520–13525.
- MATTIUSI, V., TUMMINELLO, M., IORI, G. and MANTEGNA, R. N. (2011). Comparing Correlation Matrix Estimators Via Kullback-Leibler Divergence. *Social Sciences Research Network (SSRN) Electronic Journal* 1–20.
- MEINSHAUSEN, N. and BÜHLMANN, P. (2006). High dimensional graphs and variable selection with the lasso. *The Annals of Statistics*.
- MONTI, S., CHAPUY, B., TAKEYAMA, K., RODIG, S. J., HAO, Y., YEDA, K. T., INGUILIZIAN, H., MERMEL, C., CURRIE, T., DOGAN, A. et al. (2012). Integrative analysis reveals an outcome-associated and targetable pattern of p53 and cell cycle deregulation in diffuse large B cell lymphoma. *Cancer cell* **22** 359–372.
- PETERSEN, K. and PEDERSEN, M. (2008). The Matrix Cookbook Technical University of Denmark, Technical Manual.
- PHIPSON, B. and SMYTH, G. K. (2010). Permutation P-values Should Never be Zero: Calculating Exact P-values when Permutations are Randomly Drawn. *Statistical Applications in Genetics and Molecular Biology* **9**.
- REIMAND, J., KOLDE, R. and ARAK, T. (2016). gProfileR: Interface to the 'g:Profiler' Toolkit R package version 0.6.1.
- REIMAND, J., ARAK, T., ADLER, P., KOLBERG, L., REISBERG, S., PETERSON, H. and VILO, J. (2016). g:Profiler web server for functional interpretation of gene lists (2016 update). *Nucleic Acids Research* **44** W83–W89.
- SALAVERRIA, I., PHILIPP, C., OSCHLIES, I., KOHLER, C. W., KREUZ, M., SZCZEPANOWSKI, M., BURKHARDT, B., TRAUTMANN, H., GESK, S., ANDRUSIEWICZ, M. et al. (2011). Translocations activating IRF4 identify a subtype of germinal center-derived B-cell lymphoma affecting predominantly children and young adults. *Blood* **118** 139–147.
- SHROUT, P. E. and FLEISS, J. L. (1979). Intraclass Correlations: Uses in Assessing Rater Reliability. *Psychological Bulletin* **86** 420.
- SOKAL, R. R. and ROHLF, F. J. (1962). The Comparison of Dendrograms by Objective Methods. *Taxon* **11** 33–40.
- STRONCEK, D. F., BUTTERFIELD, L. H., CANNARILE, M. A., DHODAPKAR, M. V., GRETEN, T. F., GRIVEL, J. C., KAUFMAN, D. R., KONG, H. H., KORANGY, F., LEE, P. P., MARINCOLA, F., RUTELLA, S., SIEBERT, J. C., TRINCHIERI, G. and SELIGER, B. (2017). Systematic evaluation of immune regulation and modulation. *J Immunother Cancer* **5** 21.
- R CORE TEAM (2012). R: A Language and Environment for Statistical Computing R Foundation for Statistical Computing, Vienna, Austria ISBN 3-900051-07-0.
- VAN WIERINGEN, W. N. and PEETERS, C. F. W. (2016). Ridge Estimation of Inverse Covariance Matrices from High-Dimensional Data. *Computational Statistics and Data Analysis* **103** 284–303.
- VISCO, C., LI, Y., XU-MONETTE, Z. Y., MIRANDA, R. N., GREEN, T. M., TZANKOV, A., WEN, W., LIU, W., KAHL, B., D'AMORE, E. et al. (2012). Comprehensive gene expression profiling and immunohistochemical studies support application of immunophenotypic algorithm for molecular subtype classification in diffuse large B-cell lymphoma: a report from the International DLBCL Rituximab-CHOP Consortium Program Study. *Leukemia* **26** 2103–2113.
- VON ROSEN, D. (1988). Moments for the Inverted Wishart Distribution. *Scandinavian Journal of Statistics* **15** 97–109.
- WILLIAMS, P. M., LI, R., JOHNSON, N. A., WRIGHT, G., HEATH, J.-D. and GASCOYNE, R. D. (2010). A novel method of amplification of FFPET-derived RNA enables

accurate disease classification with microarrays. *The Journal of Molecular Diagnostics* **12** 680–686.

XIE, Y. (2013). *Dynamic Documents with R and knitr*. CRC Press.

DEPARTMENT OF HAEMATOLOGY
SDR. SKOVVEJ 15
DK-9000 AALBORG
E-MAIL: anders.ellern.bilgrau@gmail.com
rfb@rn.dk
mboegsted@dcm.aau.dk
k.dybkaer@rn.dk

DEPARTMENT OF MATHEMATICAL SCIENCES
FREDRIK BAJERS VEJ 7G
DK-9220 AALBORG Ø
E-MAIL: anders.ellern.bilgrau@gmail.com
svante@math.aau.dk

DEPARTMENT OF CLINICAL MEDICINE
SDR. SKOVVEJ 15
DK-9000 AALBORG Ø
E-MAIL: mboegsted@dcm.aau.dk
k.dybkaer@rn.dk

APPENDIX A: SUPPLEMENTARY FIGURES AND TABLES

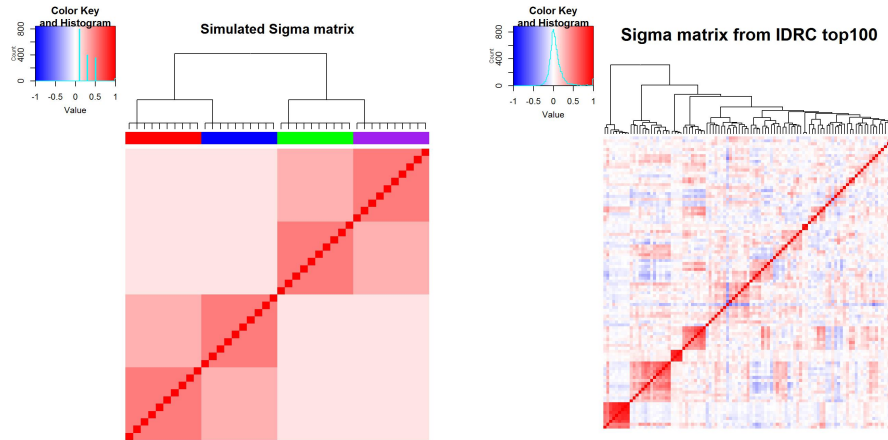


Fig A.1: Heatmaps and hierarchical clustering of the Σ matrices used for simulation.

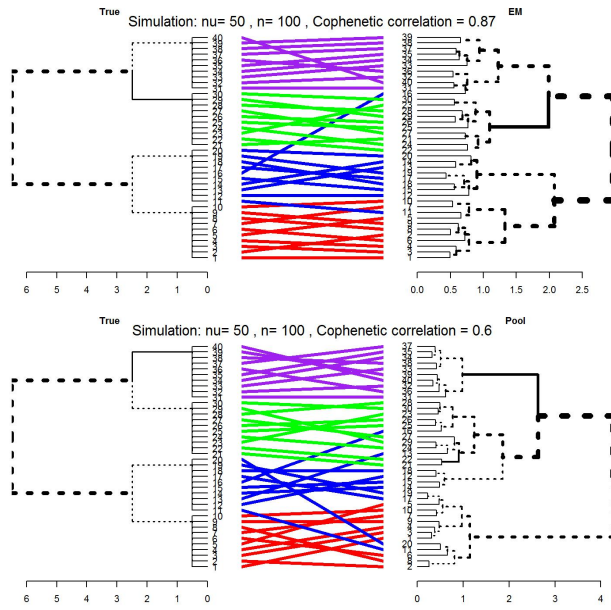


Fig A.2: Tanglegrams for the True vs estimated dendrograms with the EM and Pool method.

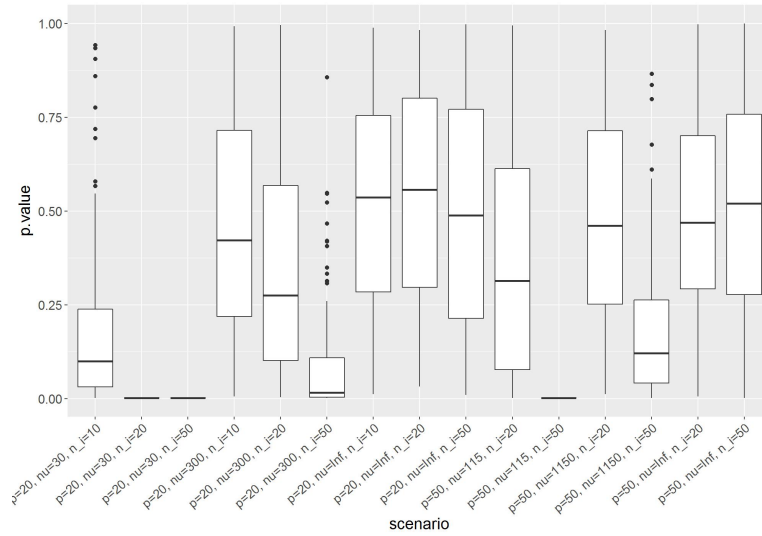


Fig A.3: Boxplot of obtained P-values from the permutation procedure under different values of p , ν and n_i .

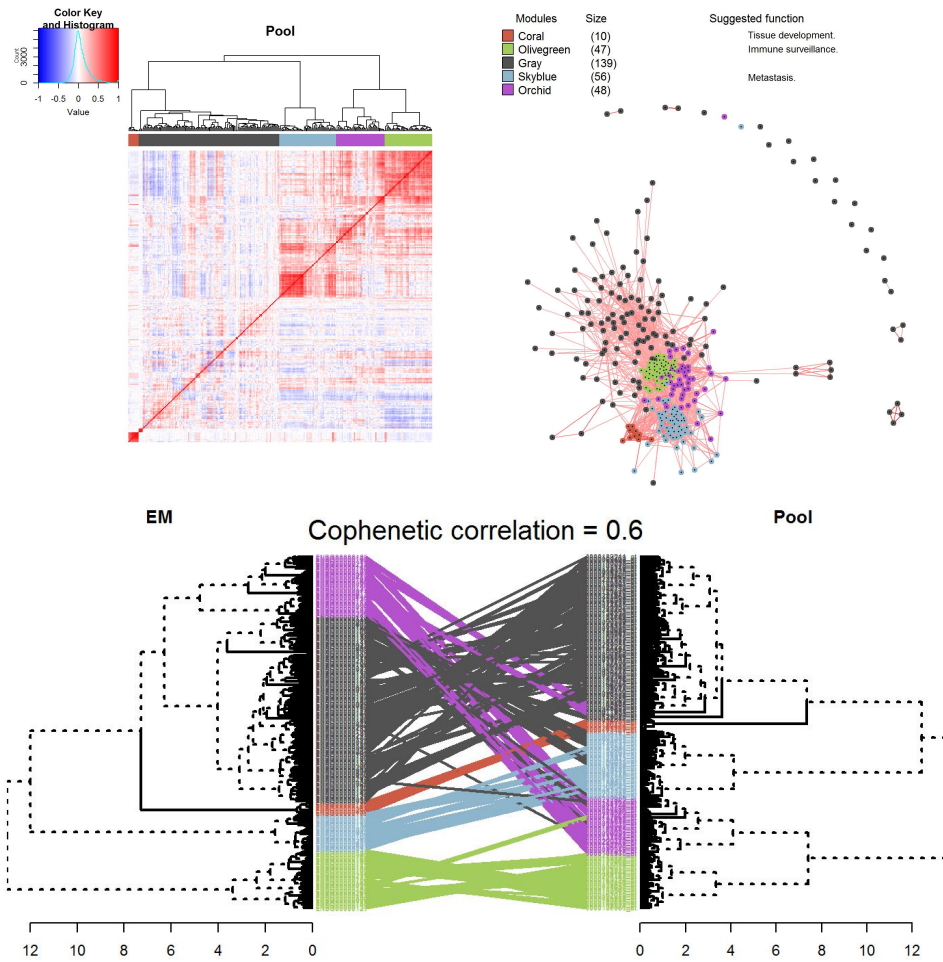


Fig A.5: Heatmap and correlation network for the estimated correlation matrices of the top 300 genes for the DLBCL data using the Pool method. The network is cut at a height producing 5 clusters. The tanglegram in the lower panel shows the comparison of clusters between the EM and Pool methods.

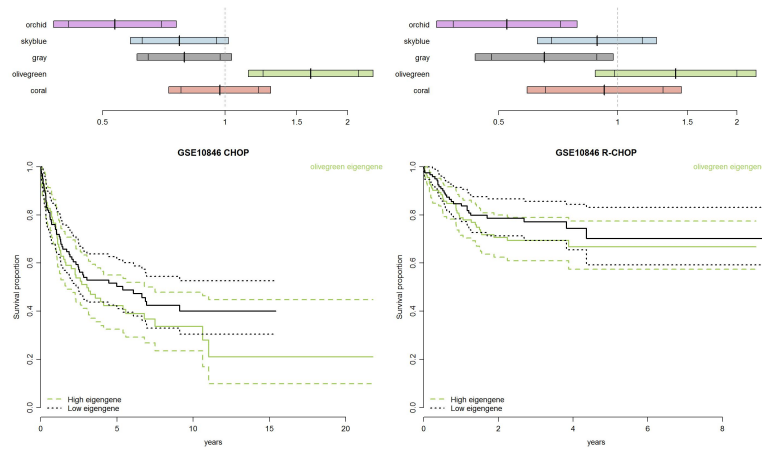


Fig A.6: The top row shows 95% and 99% CI for the hazard ratio for each eigengene in the multiple Cox proportional hazards model containing all eigengenes in the CHOP or R-CHOP dataset. The bottom row shows Kaplan-Meier estimates (and 95% CI) for the overall survival for patients stratified by the dichotomized olivegreen obtained from the Pool method. The proportion of variance explained by the eigengene in the CHOP and R-CHOP datasets for respectively the Coral, Olivegreen, Gray, Skyblue and Orchid modules were 0.72, 0.62, 0.13, 0.47, 0.33, and 0.77, 0.58, 0.13, 0.48, 0.31

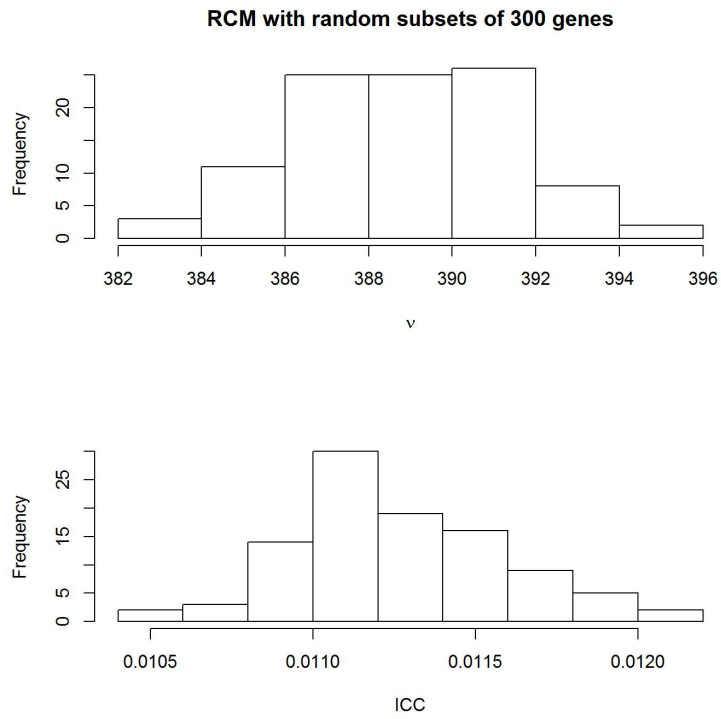


Fig A.7: Distribution of ν and the corresponding ICC when fitting the RCM with the EM method to random subsets of 300 genes.

TABLE A.1
 Mean cophenetic correlation and Kullback-Leibler divergence with 95% confidence, for estimated vs true network for different values of ν and n_i using the EM, MLE or Pool method

n_i	ν	Cophenetic Correlation			Kullback-Leibler divergence		
		EM	MLE	Pool	EM	MLE	Pool
20	50	0.19 (0.17;0.21)	0.2 (0.18;0.22)	0.2 (0.18;0.22)	236.64 (229.16;244.11)	240.37 (232.79;247.94)	227.33 (220.13;234.52)
30	50	0.26 (0.23;0.28)	0.25 (0.23;0.28)	0.25 (0.23;0.28)	123.99 (121.24;126.74)	126.61 (123.81;129.41)	121.81 (119.1;124.51)
50	50	0.6 (0.56;0.64)	0.43 (0.39;0.46)	0.43 (0.39;0.46)	44.95 (43.34;46.56)	75.62 (73.5;77.74)	73.62 (71.54;75.69)
100	50	0.88 (0.85;0.9)	0.7 (0.67;0.74)	0.7 (0.67;0.74)	13.15 (12.81;13.49)	33.04 (32.56;33.52)	30.9 (30.44;31.36)
500	50	0.99 (0.98;0.99)	0.91 (0.89;0.93)	0.91 (0.89;0.93)	7.36 (7.18;7.55)	23.64 (23.41;23.88)	21.31 (21.1;21.53)
1000	50	0.99 (0.99;0.99)	0.9 (0.88;0.92)	0.9 (0.88;0.92)	6.87 (6.69;7.06)	22.86 (22.59;23.14)	20.53 (20.28;20.78)
20	100	0.35 (0.32;0.38)	0.35 (0.32;0.37)	0.35 (0.32;0.37)	75.67 (73.06;78.28)	76.69 (74.05;79.33)	72.36 (69.85;74.86)
30	100	0.4 (0.37;0.42)	0.39 (0.37;0.42)	0.39 (0.37;0.42)	34.01 (33.27;34.75)	34.51 (33.76;35.26)	33.14 (32.42;33.87)
50	100	0.72 (0.68;0.75)	0.69 (0.66;0.72)	0.69 (0.66;0.72)	27.47 (26.75;28.18)	27.92 (27.2;28.65)	27.26 (26.55;27.97)
100	100	0.97 (0.96;0.98)	0.96 (0.95;0.97)	0.96 (0.95;0.97)	6.75 (6.62;6.88)	8.02 (7.88;8.16)	7.85 (7.71;7.98)
500	100	1 (0.99;1)	1 (1;1)	1 (1;1)	2.37 (2.35;2.4)	3.34 (3.31;3.38)	3.18 (3.15;3.21)
1000	100	1 (1;1)	1 (1;1)	1 (1;1)	2.02 (2;2.04)	2.95 (2.92;2.98)	2.79 (2.77;2.82)
20	1000	0.51 (0.48;0.54)	0.51 (0.48;0.54)	0.51 (0.48;0.54)	52.09 (50.49;53.7)	52.66 (51.04;54.29)	49.61 (48.07;51.16)
30	1000	0.61 (0.58;0.64)	0.61 (0.58;0.64)	0.61 (0.58;0.64)	22.29 (21.85;22.74)	22.5 (22.05;22.95)	21.59 (21.16;22.02)
50	1000	0.81 (0.78;0.84)	0.81 (0.78;0.84)	0.81 (0.78;0.84)	20.34 (19.76;20.92)	20.49 (19.91;21.08)	20.02 (19.44;20.59)
100	1000	0.99 (0.98;0.99)	0.99 (0.99;0.99)	0.99 (0.99;0.99)	4.41 (4.3;4.51)	4.47 (4.36;4.58)	4.42 (4.31;4.52)
500	1000	1 (1;1)	1 (1;1)	1 (1;1)	0.69 (0.68;0.7)	0.71 (0.7;0.72)	0.71 (0.7;0.72)
1000	1000	1 (1;1)	1 (1;1)	1 (1;1)	0.4 (0.4;0.41)	0.41 (0.41;0.42)	0.41 (0.4;0.42)
20	10000	0.53 (0.5;0.55)	0.52 (0.5;0.55)	0.52 (0.5;0.55)	52.58 (50.71;54.46)	53.15 (51.26;55.04)	50.07 (48.28;51.86)
30	10000	0.65 (0.61;0.68)	0.64 (0.61;0.68)	0.64 (0.61;0.68)	21.71 (21.27;22.15)	21.91 (21.46;22.35)	21.01 (20.59;21.44)
50	10000	0.83 (0.8;0.85)	0.82 (0.79;0.85)	0.82 (0.79;0.85)	19.75 (19.16;20.34)	19.88 (19.29;20.48)	19.42 (18.84;20.01)
100	10000	0.99 (0.99;1)	0.99 (0.99;1)	0.99 (0.99;1)	4.13 (4.05;4.21)	4.19 (4.11;4.27)	4.14 (4.06;4.22)
500	10000	1 (1;1)	1 (1;1)	1 (1;1)	0.58 (0.57;0.59)	0.59 (0.58;0.6)	0.59 (0.58;0.6)
1000	10000	1 (1;1)	1 (1;1)	1 (1;1)	0.27 (0.27;0.28)	0.28 (0.27;0.28)	0.28 (0.27;0.28)

TABLE A.2
Simulation results based on IDRC data. Mean cophenetic correlation and Kullback-Leibler divergence with 95% confidence, for estimated vs true network for different values of ν and n_i using the EM, MLE or Pool method.

n_i	ν	Cophenetic Correlation			Kullback-Leibler divergence		
		EM	MLE	Pool	EM	MLE	Pool
40	150	0.22 (0.2;0.25)	0.22 (0.2;0.25)	0.22 (0.2;0.25)	1420.79 (1384.39;1457.2)	1439.26 (1402.35;1476.17)	1402.29 (1366.3;1438.28)
50	150	0.25 (0.23;0.27)	0.25 (0.23;0.28)	0.25 (0.23;0.28)	647.2 (637.66;656.73)	656.21 (646.56;665.85)	642.39 (632.93;651.84)
70	150	0.3 (0.27;0.32)	0.29 (0.27;0.31)	0.29 (0.27;0.31)	383.7 (379.35;388.04)	389.72 (385.3;394.14)	383.75 (379.4;388.1)
90	150	0.32 (0.3;0.34)	0.32 (0.3;0.34)	0.32 (0.3;0.34)	306.15 (303.31;309)	311.8 (308.89;314.71)	308.05 (305.18;310.93)
150	150	0.73 (0.72;0.74)	0.65 (0.62;0.67)	0.65 (0.62;0.67)	55.57 (55.07;56.08)	82.27 (81.62;82.93)	80.52 (79.88;81.17)
500	150	0.79 (0.78;0.8)	0.76 (0.74;0.77)	0.76 (0.74;0.77)	16.82 (16.68;16.95)	31.61 (31.44;31.78)	29.51 (29.35;29.67)
1000	150	0.82 (0.81;0.84)	0.79 (0.77;0.8)	0.79 (0.77;0.8)	12.6 (12.51;12.68)	26.32 (26.19;26.45)	24.23 (24.11;24.35)
40	200	0.29 (0.26;0.32)	0.29 (0.27;0.32)	0.29 (0.27;0.32)	1025.53 (997.03;1054.02)	1038.25 (1009.41;1067.09)	1011.46 (983.34;1039.58)
50	200	0.3 (0.28;0.32)	0.29 (0.27;0.32)	0.29 (0.27;0.32)	446.39 (439.86;452.93)	452.07 (445.46;458.68)	442.48 (436;448.96)
70	200	0.36 (0.33;0.38)	0.35 (0.33;0.38)	0.35 (0.33;0.38)	258.25 (255.7;260.79)	261.7 (259.11;264.28)	257.67 (255.13;260.21)
90	200	0.38 (0.36;0.41)	0.38 (0.36;0.4)	0.38 (0.36;0.4)	203 (200.99;205.01)	205.82 (203.78;207.86)	203.34 (201.32;205.36)
150	200	0.76 (0.75;0.77)	0.72 (0.7;0.73)	0.72 (0.7;0.73)	48.6 (48.21;48.99)	58.25 (57.79;58.71)	57.71 (57.26;58.17)
500	200	0.8 (0.78;0.81)	0.8 (0.79;0.81)	0.8 (0.79;0.81)	13.45 (13.35;13.55)	18.23 (18.13;18.32)	17.41 (17.32;17.5)
1000	200	0.83 (0.82;0.84)	0.81 (0.8;0.83)	0.81 (0.8;0.83)	9.3 (9.24;9.36)	13.84 (13.78;13.91)	13.06 (13;13.12)
40	1000	0.38 (0.36;0.41)	0.38 (0.36;0.4)	0.38 (0.36;0.4)	651.25 (633.44;669.06)	658.49 (640.51;676.47)	641.33 (623.8;658.86)
50	1000	0.41 (0.39;0.44)	0.41 (0.38;0.43)	0.41 (0.38;0.43)	285.71 (281.84;289.58)	288.67 (284.77;292.57)	282.48 (278.66;286.3)
70	1000	0.46 (0.44;0.47)	0.45 (0.43;0.47)	0.45 (0.43;0.47)	161 (159.25;162.74)	162.46 (160.7;164.23)	159.95 (158.21;161.69)
90	1000	0.47 (0.45;0.49)	0.47 (0.45;0.48)	0.47 (0.45;0.48)	126.3 (125.2;127.39)	127.33 (126.22;128.43)	125.8 (124.71;126.9)
150	1000	0.74 (0.73;0.76)	0.72 (0.71;0.74)	0.72 (0.71;0.74)	38.4 (38.11;38.7)	38.96 (38.66;39.26)	38.71 (38.41;39.01)
500	1000	0.84 (0.83;0.85)	0.84 (0.83;0.85)	0.84 (0.83;0.85)	7.92 (7.87;7.98)	8.11 (8.06;8.16)	8.05 (8;8.1)
1000	1000	0.88 (0.87;0.89)	0.86 (0.85;0.87)	0.86 (0.85;0.87)	4.37 (4.34;4.4)	4.45 (4.42;4.48)	4.41 (4.38;4.44)
40	10000	0.4 (0.38;0.42)	0.4 (0.38;0.41)	0.4 (0.38;0.41)	640.15 (623.66;656.64)	647.08 (630.41;663.76)	630.21 (613.95;646.47)
50	10000	0.42 (0.4;0.44)	0.42 (0.4;0.44)	0.42 (0.4;0.44)	272.28 (268.89;275.67)	274.94 (271.52;278.37)	269.04 (265.68;272.39)
70	10000	0.46 (0.44;0.48)	0.46 (0.44;0.48)	0.46 (0.44;0.48)	153.95 (152.4;155.5)	155.23 (153.66;156.79)	152.82 (151.28;154.36)
90	10000	0.47 (0.45;0.49)	0.46 (0.45;0.48)	0.46 (0.45;0.48)	121.16 (120.12;122.2)	122.04 (121;123.09)	120.58 (119.55;121.62)
150	10000	0.75 (0.73;0.76)	0.74 (0.73;0.76)	0.74 (0.73;0.76)	36.83 (36.3;37.16)	37.21 (36.88;37.55)	36.98 (36.65;37.31)
500	10000	0.85 (0.84;0.86)	0.84 (0.83;0.86)	0.84 (0.83;0.86)	7.07 (7.03;7.12)	7.19 (7.14;7.23)	7.16 (7.12;7.21)
1000	10000	0.87 (0.86;0.88)	0.85 (0.84;0.86)	0.85 (0.84;0.86)	3.49 (3.46;3.51)	3.52 (3.49;3.54)	3.51 (3.49;3.53)

Table A.3: The significant terms for the gene enrichment , analysis of the DLBCL EM method modules. Number of genes , in each term (N), and the overlap to module (O).

Term ID	Domain	Term	P	N	O
Gray					
<i>GO</i> : 0097159	MF	organic cyclic compound bindin	$5.55e-03$	157	50
<i>GO</i> : 1901363	MF	heterocyclic compound binding	$6.64e-03$	157	48
<i>TF</i> : <i>M00940</i> ₁	tf	Factor: E2F-1; motif: NTTTCGCG	$1.50e-02$	157	34
<i>TF</i> : <i>M006950</i> ₁	tf	Factor: ETF; motif: GVGGMGG; m	$2.38e-03$	157	78
<i>TF</i> : <i>M004281</i> ₁	tf	Factor: E2F-1; motif: NKTSSCGC	$1.23e-03$	157	56
<i>TF</i> : <i>M038071</i> ₁	tf	Factor: SP2; motif: GNNGGGGGCG	$4.27e-02$	157	40
<i>TF</i> : <i>M011990</i> ₁	tf	Factor: RNF96; motif: BCCCGCRG	$3.63e-02$	157	65
<i>TF</i> : <i>M011991</i> ₁	tf	Factor: RNF96; motif: BCCCGCRG	$4.27e-02$	157	40
<i>TF</i> : <i>M048690</i> ₁	tf	Factor: Egr-1; motif: GCGCATGC	$2.42e-02$	157	99
<i>TF</i> : <i>M048691</i> ₁	tf	Factor: Egr-1; motif: GCGCATGC	$1.87e-03$	157	88
<i>TF</i> : <i>M072501</i> ₁	tf	Factor: E2F-1; motif: NNNSSCGC	$3.95e-02$	157	54
<i>TF</i> : <i>M088741</i> ₁	tf	Factor: E2F1; motif: NNNNGCGS	$1.61e-02$	157	36
<i>TF</i> : <i>M008031</i> ₁	tf	Factor: E2F; motif: GCGGSG; ma	$3.88e-04$	157	87
<i>TF</i> : <i>M009381</i> ₁	tf	Factor: E2F-1; motif: TTGGGCGC	$5.69e-03$	157	40
<i>TF</i> : <i>M020900</i> ₁	tf	Factor: E2F-4; motif: GCGGAAA	$1.38e-02$	157	117
Olivegreen					
<i>GO</i> : 0006952	BP	defense response	$7.88e-04$	48	29
<i>GO</i> : 0045087	BP	innate immune response	$3.99e-04$	48	20
<i>GO</i> : 0045088	BP	regulation of innate immune re	$2.33e-02$	48	10
<i>GO</i> : 0009615	BP	response to virus	$4.94e-02$	48	9
<i>GO</i> : 0009607	BP	response to biotic stimulus	$2.64e-02$	48	18
<i>REAC</i> : 5660526	rea	Response to metal ions	$5.00e-02$	48	4
<i>REAC</i> : 5661231	rea	Metallothioneins bind metals	$5.00e-02$	48	4
Orchid					
<i>GO</i> : 0002376	BP	immune system process	$2.90e-02$	49	36
<i>GO</i> : 0006644	BP	phospholipid metabolic process	$1.83e-02$	49	8
<i>REAC</i> : 2730905	rea	Role of LAT2/NTAL/LAB on calci	$1.08e-02$	49	5
<i>REAC</i> : 2029482	rea	Regulation of actin dynamics f	$4.98e-02$	49	4
<i>REAC</i> : 2029485	rea	Role of phospholipids in phago	$4.98e-02$	49	4
<i>REAC</i> : 2871809	rea	FCERI mediated Ca+2 mobilizati	$1.08e-02$	49	5
<i>REAC</i> : 2871837	rea	FCERI mediated NF-kB activatio	$4.98e-02$	49	4

Table A.3: (continued)

Term ID	Domain	Term	P	N	O
Skyblue					
GO : 0009719	BP	response to endogenous stimulu	8.88e - 03	31	12
GO : 0009611	BP	response to wounding	4.05e - 03	31	12
GO : 0042060	BP	wound healing	9.50e - 03	31	11
GO : 0071230	BP	cellular response to amino aci	2.58e - 02	31	5
GO : 0032502	BP	developmental process	1.34e - 02	31	26
GO : 0048856	BP	anatomical structure developme	2.78e - 03	31	26
GO : 0009888	BP	tissue development	1.16e - 02	31	16
GO : 0009653	BP	anatomical structure morphogen	2.64e - 03	31	18
GO : 0051093	BP	negative regulation of develop	1.07e - 03	31	12
GO : 0048646	BP	anatomical structure formation	3.52e - 02	31	12
GO : 0044767	BP	single-organism developmental	9.58e - 03	31	26
GO : 0007275	BP	multicellular organism develop	4.02e - 04	31	26
GO : 0048731	BP	system development	2.28e - 03	31	24
GO : 0072359	BP	circulatory system development	1.83e - 04	31	14
GO : 0001501	BP	skeletal system development	8.37e - 09	31	15
GO : 0072358	BP	cardiovascular system developm	2.66e - 03	31	12
GO : 0001944	BP	vasculature development	2.66e - 03	31	12
GO : 0001568	BP	blood vessel development	2.66e - 03	31	12
GO : 0010243	BP	response to organonitrogen com	3.02e - 02	31	9
GO : 0032501	BP	multicellular organismal proce	2.06e - 02	31	28
GO : 0071840	BP	cellular component organizatio	1.36e - 03	31	25
GO : 0016043	BP	cellular component organizatio	1.11e - 03	31	25
GO : 0043062	BP	extracellular structure organi	1.77e - 13	31	20
GO : 0030198	BP	extracellular matrix organizat	1.77e - 13	31	20
GO : 0030199	BP	collagen fibril organization	1.13e - 03	31	7
GO : 0050953	BP	sensory perception of light st	4.98e - 02	31	4
GO : 0007601	BP	visual perception	4.98e - 02	31	4
GO : 0009056	BP	catabolic process	6.84e - 03	31	16
GO : 0044712	BP	single-organism catabolic proc	1.14e - 04	31	14
GO : 0044236	BP	multicellular organism metabol	2.82e - 05	31	11
GO : 0044243	BP	multicellular organismal catab	1.48e - 06	31	11
GO : 0044259	BP	multicellular organismal macro	2.82e - 05	31	11
GO : 0032963	BP	collagen metabolic process	2.82e - 05	31	11
GO : 0030574	BP	collagen catabolic process	1.48e - 06	31	11
GO : 0012505	CC	endomembrane system	1.91e - 03	31	23
GO : 0005576	CC	extracellular region	2.40e - 03	31	28
GO : 0099080	CC	supramolecular complex	2.43e - 03	31	11
GO : 0099081	CC	supramolecular polymer	2.43e - 03	31	11
GO : 0099512	CC	supramolecular fiber	2.43e - 03	31	11
GO : 0044421	CC	extracellular region part	1.18e - 04	31	28
GO : 0005615	CC	extracellular space	9.33e - 06	31	25
GO : 0031012	CC	extracellular matrix	4.04e - 10	31	19
GO : 0044420	CC	extracellular matrix component	6.83e - 12	31	13
GO : 0005578	CC	proteinaceous extracellular ma	3.49e - 11	31	18
GO : 0005604	CC	basement membrane	3.66e - 05	31	7
GO : 0043234	CC	protein complex	2.49e - 03	31	13
GO : 0005581	CC	collagen trimer	4.24e - 07	31	11
GO : 0098644	CC	complex of collagen trimers	3.66e - 05	31	7
GO : 0098643	CC	banded collagen fibril	3.66e - 05	31	7
GO : 0005583	CC	fibrillar collagen trimer	3.66e - 05	31	7
GO : 0044432	CC	endoplasmic reticulum part	8.73e - 03	31	10
GO : 0005788	CC	endoplasmic reticulum lumen	2.57e - 05	31	8
GO : 0050840	MF	extracellular matrix binding	2.58e - 02	31	5
GO : 0048407	MF	platelet-derived growth factor	4.98e - 02	31	4
GO : 0043169	MF	cation binding	1.18e - 03	31	18
GO : 0046872	MF	metal ion binding	4.93e - 04	31	18
GO : 0005201	MF	extracellular matrix structura	1.18e - 05	31	9
GO : 0044877	MF	macromolecular complex binding	3.26e - 02	31	10
GO : 0032403	MF	protein complex binding	2.16e - 02	31	10
HP : 0000002	hp	Abnormality of body height	4.37e - 02	31	12
KEGG : 04510	keg	Focal adhesion	4.99e - 02	31	5
KEGG : 04974	keg	Protein digestion and absorpti	4.45e - 04	31	8
KEGG : 04512	keg	ECM-receptor interaction	1.65e - 02	31	5
REAC : 3781865	rea	Diseases of glycosylation	7.07e - 03	31	4
REAC : 1474244	rea	Extracellular matrix organizat	6.26e - 11	31	17
REAC : 3000178	rea	ECM proteoglycans	7.07e - 03	31	4
REAC : 1474228	rea	Degradation of the extracellul	3.07e - 02	31	6
REAC : 1474290	rea	Collagen formation	2.98e - 05	31	9
REAC : 2022090	rea	Assembly of collagen fibrils a	1.97e - 04	31	8
REAC : 1650814	rea	Collagen biosynthesis and modi	1.85e - 07	31	9

Table A.3: (continued)

Term ID	Domain	Term	P	N	O
Coral					
GO : 0009888	BP	tissue development	1.02e - 03	10	9
GO : 0060429	BP	epithelium development	7.35e - 07	10	9
GO : 0030855	BP	epithelial cell differentiatio	1.01e - 08	10	9
GO : 0008544	BP	epidermis development	2.23e - 10	10	9
GO : 0009913	BP	epidermal cell differentiation	2.47e - 11	10	9
GO : 0008219	BP	cell death	3.95e - 03	10	9
GO : 0012501	BP	programmed cell death	2.22e - 03	10	9
GO : 0043588	BP	skin development	5.35e - 09	10	9
GO : 0030216	BP	keratinocyte differentiation	2.47e - 11	10	9
GO : 0031424	BP	keratinization	1.13e - 12	10	9
GO : 0070268	BP	cornification	1.44e - 10	10	8
GO : 0018149	BP	peptide cross-linking	3.55e - 02	10	4
GO : 0099513	CC	polymeric cytoskeletal fiber	4.54e - 03	10	5
GO : 0045111	CC	intermediate filament cytoskel	3.76e - 05	10	5
GO : 0005882	CC	intermediate filament	6.36e - 06	10	5
GO : 0045095	CC	keratin filament	3.06e - 04	10	4
GO : 0001533	CC	cornified envelope	4.44e - 03	10	4
GO : 0005198	MF	structural molecule activity	4.41e - 05	10	8
GO : 0005200	MF	structural constituent of cyto	2.00e - 02	10	4
HPA : 053030_01	hpa	tonsil; squamous epithelial ce	9.03e - 03	10	9
HPA : 053030_02	hpa	tonsil; squamous epithelial ce	1.63e - 04	10	9
HPA : 053030_01_1	hpa	tonsil; squamous epithelial ce	7.87e - 05	10	9
HPA : 053030_01_2	hpa	tonsil; squamous epithelial ce	2.70e - 06	10	9
HPA : 029010_01	hpa	oral mucosa; squamous epitheli	2.59e - 03	10	9
HPA : 029010_02	hpa	oral mucosa; squamous epitheli	8.70e - 04	10	8
HPA : 029010_03	hpa	oral mucosa; squamous epitheli	9.38e - 03	10	5
HPA : 029010_01_1	hpa	oral mucosa; squamous epitheli	3.54e - 05	10	9
HPA : 029010_01_2	hpa	oral mucosa; squamous epitheli	8.81e - 05	10	8
HPA : 029010_01_3	hpa	oral mucosa; squamous epitheli	9.38e - 03	10	5
HPA : 015010_01	hpa	esophagus; squamous epithelial	3.06e - 03	10	9
HPA : 015010_02	hpa	esophagus; squamous epithelial	1.29e - 04	10	9
HPA : 015010_03	hpa	esophagus; squamous epithelial	9.55e - 05	10	7
HPA : 015010_01_1	hpa	esophagus; squamous epithelial	4.66e - 05	10	9
HPA : 015010_01_2	hpa	esophagus; squamous epithelial	1.84e - 06	10	9
HPA : 015010_01_3	hpa	esophagus; squamous epithelial	3.52e - 05	10	7
HPA : 009020_01	hpa	cervix, uterine; squamous epit	1.46e - 02	10	8
HPA : 009020_02	hpa	cervix, uterine; squamous epit	3.99e - 04	10	8
HPA : 009020_03	hpa	cervix, uterine; squamous epit	1.30e - 03	10	6
HPA : 009020_01_1	hpa	cervix, uterine; squamous epit	3.02e - 04	10	8
HPA : 009020_01_2	hpa	cervix, uterine; squamous epit	1.33e - 05	10	8
HPA : 009020_01_3	hpa	cervix, uterine; squamous epit	8.27e - 04	10	6
HPA : 042030_01_1	hpa	skin 1; keratinocytes[Supporte	1.62e - 02	10	7
HPA : 042030_01_2	hpa	skin 1; keratinocytes[Supporte	8.13e - 03	10	6
HPA : 055010_01	hpa	vagina; squamous epithelial ce	1.07e - 03	10	9
HPA : 055010_02	hpa	vagina; squamous epithelial ce	1.47e - 05	10	9
HPA : 055010_03	hpa	vagina; squamous epithelial ce	3.00e - 02	10	5
HPA : 055010_01_1	hpa	vagina; squamous epithelial ce	7.76e - 06	10	9
HPA : 055010_01_2	hpa	vagina; squamous epithelial ce	1.99e - 07	10	9
HPA : 055010_01_3	hpa	vagina; squamous epithelial ce	2.11e - 02	10	5
HPA : 043010_03	hpa	skin 2; epidermal cells[Uncert	9.38e - 03	10	5
HPA : 043010_01_1	hpa	skin 2; epidermal cells[Suppor	2.19e - 03	10	8
HPA : 043010_01_2	hpa	skin 2; epidermal cells[Suppor	1.46e - 02	10	6
HPA : 043010_01_3	hpa	skin 2; epidermal cells[Suppor	9.38e - 03	10	5
OMIM : 131800	omi	EPIDERMOLYSIS BULLOSA SIMPLEX,	5.00e - 02	10	2
OMIM : 601001	omi	EPIDERMOLYSIS BULLOSA SIMPLEX,	5.00e - 02	10	2
OMIM : 131760	omi	EPIDERMOLYSIS BULLOSA SIMPLEX,	5.00e - 02	10	2
OMIM : 131900	omi	EPIDERMOLYSIS BULLOSA SIMPLEX,	5.00e - 02	10	2
REAC : 1266738	rea	Developmental Biology	8.62e - 07	10	8
TF : M07051_1	tf	Factor: NF-1B; motif: CTGGCAG	6.22e - 03	10	7

Table A.5: (*continued*)

Term ID	Domain	Term	P	N	O
---------	--------	------	---	---	---

Table A.5: The significant terms for the gene enrichment , analysis of the DLBCL Pool method modules. Number of genes , in each term (N), and the overlap to module (O).

Term ID	Domain	Term	P	N	O
Gray					
<i>TF</i> : M00940 ₁	tf	Factor: E2F-1; motif: NTTTCGCG	$3.04e - 02$	136	31
Olivegreen					
<i>GO</i> : 0006952	BP	defense response	$2.10e - 03$	45	27
<i>GO</i> : 0045087	BP	innate immune response	$5.53e - 04$	45	19
<i>GO</i> : 0045088	BP	regulation of innate immune re	$9.89e - 03$	45	10
<i>REAC</i> : 5660526	rea	Response to metal ions	$4.98e - 02$	45	4
<i>REAC</i> : 5661231	rea	Metallothioneins bind metals	$4.98e - 02$	45	4

Table A.5: (continued)

Term ID	Domain	Term	P	N	O
Skyblue					
GO : 0051093	BP	negative regulation of develop	2.67e - 02	56	14
GO : 0007167	BP	enzyme linked receptor protein	8.80e - 03	56	14
GO : 0007178	BP	transmembrane receptor protein	2.54e - 03	56	8
GO : 0007517	BP	muscle organ development	4.98e - 02	56	9
GO : 0010243	BP	response to organonitrogen com	1.71e - 02	56	12
GO : 0043200	BP	response to amino acid	1.32e - 02	56	7
GO : 0032501	BP	multicellular organismal proce	2.68e - 02	56	45
GO : 0044707	BP	single-multicellular organism	4.07e - 02	56	44
GO : 0001503	BP	ossification	4.02e - 03	56	12
GO : 0044712	BP	single-organism catabolic proc	2.06e - 03	56	17
GO : 0044236	BP	multicellular organism metabol	9.61e - 06	56	14
GO : 0044243	BP	multicellular organismal catab	6.82e - 05	56	12
GO : 0044259	BP	multicellular organismal macro	9.61e - 06	56	14
GO : 0032963	BP	collagen metabolic process	9.61e - 06	56	14
GO : 0030574	BP	collagen catabolic process	6.82e - 05	56	12
GO : 0070848	BP	response to growth factor	1.28e - 04	56	15
GO : 0071363	BP	cellular response to growth fa	5.43e - 04	56	14
GO : 0009653	BP	anatomical structure morphogen	8.62e - 03	56	25
GO : 0048646	BP	anatomical structure formation	1.54e - 02	56	17
GO : 0072359	BP	circulatory system development	8.14e - 05	56	19
GO : 0072358	BP	cardiovascular system developm	3.32e - 04	56	17
GO : 0001944	BP	vasculature development	3.32e - 04	56	17
GO : 0009887	BP	animal organ morphogenesis	2.44e - 03	56	14
GO : 0001568	BP	blood vessel development	3.32e - 04	56	17
GO : 0048514	BP	blood vessel morphogenesis	4.75e - 03	56	14
GO : 0001525	BP	angiogenesis	1.69e - 02	56	13
GO : 0071822	BP	protein complex subunit organi	1.17e - 02	56	16
GO : 0071840	BP	cellular component organizatio	2.24e - 03	56	38
GO : 0016043	BP	cellular component organizatio	1.71e - 03	56	38
GO : 0097435	BP	supramolecular fiber organizat	1.28e - 04	56	15
GO : 0043062	BP	extracellular structure organi	1.19e - 13	56	25
GO : 0030198	BP	extracellular matrix organizat	1.19e - 13	56	25
GO : 0030199	BP	collagen fibril organization	5.59e - 05	56	9
GO : 0009888	BP	tissue development	3.46e - 02	56	22
GO : 0061448	BP	connective tissue development	2.97e - 03	56	11
GO : 0001501	BP	skeletal system development	1.84e - 09	56	19
GO : 0051216	BP	cartilage development	4.43e - 04	56	10
GO : 0009611	BP	response to wounding	6.33e - 04	56	17
GO : 0042060	BP	wound healing	4.54e - 03	56	15
GO : 0009719	BP	response to endogenous stimulu	4.15e - 05	56	19
GO : 0071495	BP	cellular response to endogenou	2.93e - 04	56	15
GO : 0005576	CC	extracellular region	2.53e - 04	56	46
GO : 0044421	CC	extracellular region part	2.09e - 06	56	46
GO : 0005615	CC	extracellular space	1.76e - 06	56	38
GO : 0031012	CC	extracellular matrix	8.36e - 11	56	25
GO : 0044420	CC	extracellular matrix component	3.76e - 08	56	13
GO : 0005578	CC	proteinaceous extracellular ma	5.45e - 12	56	23
GO : 0005604	CC	basement membrane	1.94e - 03	56	7
GO : 0005581	CC	collagen trimer	3.40e - 04	56	11
GO : 0098644	CC	complex of collagen trimers	1.94e - 03	56	7
GO : 0098643	CC	banded collagen fibril	1.94e - 03	56	7
GO : 0005583	CC	fibrillar collagen trimer	1.94e - 03	56	7
GO : 0012505	CC	endomembrane system	1.71e - 02	56	33
GO : 0005788	CC	endoplasmic reticulum lumen	2.54e - 03	56	8
GO : 0032403	MF	protein complex binding	3.00e - 02	56	13
GO : 0043167	MF	ion binding	4.41e - 02	56	32
GO : 0043169	MF	cation binding	1.24e - 02	56	24
GO : 0046872	MF	metal ion binding	4.34e - 03	56	24
GO : 0005201	MF	extracellular matrix structura	8.67e - 05	56	10
GO : 0050840	MF	extracellular matrix binding	1.11e - 02	56	6
KEGG : 04933	keg	AGE-RAGE signaling pathway in	1.62e - 02	56	6
KEGG : 04974	keg	Protein digestion and absorpti	3.86e - 02	56	8
REAC : 1474244	rea	Extracellular matrix organizat	7.33e - 07	56	18
REAC : 1474290	rea	Collagen formation	6.62e - 03	56	9
REAC : 1650814	rea	Collagen biosynthesis and modi	6.07e - 05	56	9
REAC : 2022090	rea	Assembly of collagen fibrils a	2.10e - 02	56	8
Orchid					
GO : 0042581	CC	specific granule	4.55e - 02	48	6
GO : 0035580	CC	specific granule lumen	4.55e - 02	48	6

Table A.5: (continued)

Term ID	Domain	Term	P	N	O
Coral					
GO : 0009888	BP	tissue development	1.02e - 03	10	9
GO : 0008544	BP	epidermis development	2.23e - 10	10	9
GO : 0060429	BP	epithelium development	7.35e - 07	10	9
GO : 0030855	BP	epithelial cell differentiatio	1.01e - 08	10	9
GO : 0009913	BP	epidermal cell differentiation	2.47e - 11	10	9
GO : 0008219	BP	cell death	3.95e - 03	10	9
GO : 0012501	BP	programmed cell death	2.22e - 03	10	9
GO : 0043588	BP	skin development	5.35e - 09	10	9
GO : 0030216	BP	keratinocyte differentiation	2.47e - 11	10	9
GO : 0031424	BP	keratinization	1.13e - 12	10	9
GO : 0070268	BP	cornification	1.44e - 10	10	8
GO : 0018149	BP	peptide cross-linking	3.55e - 02	10	4
GO : 0001533	CC	cornified envelope	4.44e - 03	10	4
GO : 0099513	CC	polymeric cytoskeletal fiber	4.54e - 03	10	5
GO : 0045111	CC	intermediate filament cytoskel	3.76e - 05	10	5
GO : 0005882	CC	intermediate filament	6.36e - 06	10	5
GO : 0045095	CC	keratin filament	3.06e - 04	10	4
GO : 0005198	MF	structural molecule activity	4.41e - 05	10	8
GO : 0005200	MF	structural constituent of cyto	2.00e - 02	10	4
HPA : 009020 ₀ 1	hpa	cervix, uterine; squamous epit	1.46e - 02	10	8
HPA : 009020 ₀ 2	hpa	cervix, uterine; squamous epit	3.99e - 04	10	8
HPA : 009020 ₀ 3	hpa	cervix, uterine; squamous epit	1.30e - 03	10	6
HPA : 009020 ₁ 1	hpa	cervix, uterine; squamous epit	3.02e - 04	10	8
HPA : 009020 ₁ 2	hpa	cervix, uterine; squamous epit	1.33e - 05	10	8
HPA : 009020 ₁ 3	hpa	cervix, uterine; squamous epit	8.27e - 04	10	6
HPA : 053030 ₀ 1	hpa	tonsil; squamous epithelial ce	9.03e - 03	10	9
HPA : 053030 ₀ 2	hpa	tonsil; squamous epithelial ce	1.63e - 04	10	9
HPA : 053030 ₁ 1	hpa	tonsil; squamous epithelial ce	7.87e - 05	10	9
HPA : 053030 ₁ 2	hpa	tonsil; squamous epithelial ce	2.70e - 06	10	9
HPA : 055010 ₀ 1	hpa	vagina; squamous epithelial ce	1.07e - 03	10	9
HPA : 055010 ₀ 2	hpa	vagina; squamous epithelial ce	1.47e - 05	10	9
HPA : 055010 ₀ 3	hpa	vagina; squamous epithelial ce	3.00e - 02	10	5
HPA : 055010 ₁ 1	hpa	vagina; squamous epithelial ce	7.76e - 06	10	9
HPA : 055010 ₁ 2	hpa	vagina; squamous epithelial ce	1.99e - 07	10	9
HPA : 055010 ₁ 3	hpa	vagina; squamous epithelial ce	2.11e - 02	10	5
HPA : 029010 ₀ 1	hpa	oral mucosa; squamous epitheli	2.59e - 03	10	9
HPA : 029010 ₀ 2	hpa	oral mucosa; squamous epitheli	8.70e - 04	10	8
HPA : 029010 ₀ 3	hpa	oral mucosa; squamous epitheli	9.38e - 03	10	5
HPA : 029010 ₁ 1	hpa	oral mucosa; squamous epitheli	3.54e - 05	10	9
HPA : 029010 ₁ 2	hpa	oral mucosa; squamous epitheli	8.81e - 05	10	8
HPA : 029010 ₁ 3	hpa	oral mucosa; squamous epitheli	9.38e - 03	10	5
HPA : 043010 ₀ 3	hpa	skin 2; epidermal cells[Uncert	9.38e - 03	10	5
HPA : 043010 ₁ 1	hpa	skin 2; epidermal cells[Suppor	2.19e - 03	10	8
HPA : 043010 ₁ 2	hpa	skin 2; epidermal cells[Suppor	1.46e - 02	10	6
HPA : 043010 ₁ 3	hpa	skin 2; epidermal cells[Suppor	9.38e - 03	10	5
HPA : 015010 ₀ 1	hpa	esophagus; squamous epithelial	3.06e - 03	10	9
HPA : 015010 ₀ 2	hpa	esophagus; squamous epithelial	1.29e - 04	10	9
HPA : 015010 ₀ 3	hpa	esophagus; squamous epithelial	9.55e - 05	10	7
HPA : 015010 ₁ 1	hpa	esophagus; squamous epithelial	4.66e - 05	10	9
HPA : 015010 ₁ 2	hpa	esophagus; squamous epithelial	1.84e - 06	10	9
HPA : 015010 ₁ 3	hpa	esophagus; squamous epithelial	3.52e - 05	10	7
HPA : 042030 ₁ 1	hpa	skin 1; keratinocytes[Supporte	1.62e - 02	10	7
HPA : 042030 ₁ 2	hpa	skin 1; keratinocytes[Supporte	8.13e - 03	10	6
OMIM : 601001	omi	EPIDERMOLYSIS BULLOSA SIMPLEX,	5.00e - 02	10	2
OMIM : 131760	omi	EPIDERMOLYSIS BULLOSA SIMPLEX,	5.00e - 02	10	2
OMIM : 131900	omi	EPIDERMOLYSIS BULLOSA SIMPLEX,	5.00e - 02	10	2
OMIM : 131800	omi	EPIDERMOLYSIS BULLOSA SIMPLEX,	5.00e - 02	10	2
REAC : 1266738	rea	Developmental Biology	8.62e - 07	10	8
TF : M07051 ₁	tf	Factor: NF-1B; motif: CTGGCASC	6.22e - 03	10	7

Gray n = 139	Olivegreen n = 47	Skyblue n = 56	Orchid n = 48	Coral n = 10
MYBL1	FCER1G	COL5A2	CD2	KRT6A
BATF	C1QB	COL1A2	PTGDS	SPRR1A
STAP1	IDO1	COL3A1	GIMAP4	SPRR1B
MME	GBP1	VCAN	ADAMDEC1	SPRR3
CD44	C1QA	DCN	CD3D	S100A2
CYB5R2	CD14	COL6A3	CCL19	KRT13
TNFRSF13B	GZMA	THBS2	IL18	KRT14
LRMP	SERPING1	SPARC	TFEC	DSP
MARCKSL1	RARRES3	SULF1	ITK	KRT5
BCL2A1	CXCL10	MMP2	PLA2G2D	
HCK	PSTPIP2	MXRA5	APOC1	
CCND2	GBP2	LUM	CHI3L1	
VPREB3	FGL2	CTGF	LYZ	
LMO2	CXCL11	COL15A1	ENPP2	
HLA-DOB	CCL8	COL5A1	LGALS2	
STAG3	LILRB2	FAP	CSTA	
PDGFD	CXCL9	COL1A1	CXCL13	
CCR7	CD163	POSTN	ITM2A	
BLNK	GZMB	TMEM45A	CLU	
SORL1	GZMH	EMP1	PLA2G7	
MNDA	GZMK	CTSK	IL7R	
RRAS2	ALDH1A1	PLS3	TRBC2	
SPINK2	IFNG	TGFBI	HSD11B1	
BACH2	SLAMF7	GJA1	MMP9	
NCF2	CPVL	COL11A1	C3	
GPR183	KCNJ2	AEBP1	CXCL14	
OSBPL10	CD8A	TIMP1	CYP27B1	
GRHPR	MS4A4A	TNFAIP6	CHIT1	
DUSP5	MT1G	ANXA1	LAMP3	
ALOX5AP	LGMN	TAGLN	CCL21	
CD22	MT2A	FOS	ROBO1	
MS4A1	IGSF6	CILP	MAL	
SYBU	S100A8	DPT	KLRB1	
TCL1A	CRTAM	MGP	SQOR	
FCMR	GNLY	SPP1	ORM1	
GPR137B	S100A9	GOS2	SELENOP	
IGHM	GPX3	STEAP1	P2RY14	
SLC12A8	MT1M	MMP1	NPY1R	
CD83	PLTP	EPS8	ORM2	
GMDS	MARCO	GREM1	TRDC	

TABLE A.4

The identified modules from the Pool method, their sizes, and member genes. The genes are sorted decreasingly by their intra-module connectivity (sum of the incident edge weights). Only the top 40 genes are shown.

APPENDIX B: MARGINALIZATION OF THE COVARIANCE

This section shows the marginalization over Σ in (2.3). Recall the model (2.1) where $\mathcal{N}_p(\boldsymbol{\mu}, \Sigma_i)$ denotes a p -dimensional multivariate Gaussian distribution with mean $\boldsymbol{\mu}$ and positive definite (p.d.) covariance matrix Σ_i with probability density function (pdf)

$$(B.1) \quad f(\mathbf{x}|\boldsymbol{\mu}, \Sigma_i) = (2\pi)^{-\frac{p}{2}} |\Sigma_i|^{-\frac{1}{2}} \exp\left(-\frac{1}{2}(\mathbf{x} - \boldsymbol{\mu})^\top \Sigma_i^{-1}(\mathbf{x} - \boldsymbol{\mu})\right),$$

and where $\mathcal{W}_p^{-1}(\Psi, \nu)$ denotes a p -dimensional inverse Wishart distribution with ν degrees of freedom, a p.d. $p \times p$ scale matrix Ψ , and pdf

$$(B.2) \quad f(\Sigma_i) = \frac{|\Psi|^{\frac{\nu}{2}}}{2^{\frac{\nu p}{2}} \Gamma_p\left(\frac{\nu}{2}\right)} |\Sigma_i|^{-\frac{\nu+p+1}{2}} \exp\left(-\frac{1}{2} \text{tr}(\Psi \Sigma_i^{-1})\right), \quad \nu > p - 1,$$

where Σ_i is p.d. and Γ_p is the multivariate generalization of the gamma function Γ given by

$$(B.3) \quad \Gamma_p(t) = \pi^{\frac{1}{2} \binom{p}{2}} \prod_{j=1}^p \Gamma\left(t + \frac{1-j}{2}\right) \quad \text{where } \Gamma(t) = \int_0^\infty x^{t-1} e^{-x} dx.$$

For ease of notation we drop the subscript i on Σ_i , \mathbf{X}_i , $\mathbf{S}_i = \mathbf{X}_i \mathbf{X}_i^\top$, and n_i . By the model assumptions,

$$\begin{aligned} f(\mathbf{X}|\Psi, \nu) &= \int f(\mathbf{X}|\Sigma) f(\Sigma|\Psi, \nu) d\Sigma \\ &= \int \left[\prod_{j=1}^n (2\pi)^{-\frac{p}{2}} |\Sigma|^{-\frac{1}{2}} e^{-\frac{1}{2} \text{tr}(\mathbf{x}_{ij} \mathbf{x}_{ij}^\top \Sigma^{-1})} \right] \frac{|\Psi|^{\frac{\nu}{2}}}{2^{\frac{\nu p}{2}} \Gamma_p\left(\frac{\nu}{2}\right)} |\Sigma|^{-\frac{\nu+p+1}{2}} e^{-\frac{1}{2} \text{tr}(\Psi \Sigma^{-1})} d\Sigma \\ &= (2\pi)^{-\frac{np}{2}} \frac{|\Psi|^{\frac{\nu}{2}}}{2^{\frac{\nu p}{2}} \Gamma_p\left(\frac{\nu}{2}\right)} \int |\Sigma|^{-\frac{n}{2}} e^{-\frac{1}{2} \text{tr}(\mathbf{S} \Sigma^{-1})} |\Sigma|^{-\frac{\nu+p+1}{2}} e^{-\frac{1}{2} \text{tr}(\Psi \Sigma^{-1})} d\Sigma \\ &= \frac{|\Psi|^{\frac{\nu}{2}}}{\pi^{\frac{np}{2}} 2^{\frac{(\nu+n)p}{2}} \Gamma_p\left(\frac{\nu}{2}\right)} \int |\Sigma|^{-\frac{(\nu+n)+p+1}{2}} e^{-\frac{1}{2} \text{tr}((\Psi + \mathbf{S}) \Sigma^{-1})} d\Sigma. \end{aligned}$$

The integrand can be recognized as a unnormalized inverse Wishart pdf of the distribution $\mathcal{W}^{-1}(\Psi + \mathbf{S}, \nu + n)$, and so the integral evaluates to the reciprocal value of the normalizing constant in that density. Thus,

$$(B.4) \quad f(\mathbf{X}|\Psi, \nu) = \frac{|\Psi|^{\frac{\nu}{2}}}{\pi^{\frac{np}{2}} 2^{\frac{(\nu+n)p}{2}} \Gamma_p\left(\frac{\nu}{2}\right)} \frac{2^{\frac{(\nu+n)p}{2}} \Gamma_p\left(\frac{\nu+n}{2}\right)}{|\Psi + \mathbf{S}|^{\frac{\nu+n}{2}}} = \frac{|\Psi|^{\frac{\nu}{2}} \Gamma_p\left(\frac{\nu+n}{2}\right)}{\pi^{\frac{np}{2}} |\Psi + \mathbf{S}|^{\frac{\nu+n}{2}} \Gamma_p\left(\frac{\nu}{2}\right)}.$$

Using the matrix determinant lemma and $\mathbf{S} = \mathbf{X}^\top \mathbf{X}$, this can be further simplified to

$$f(\mathbf{X}|\boldsymbol{\Psi}, \nu) = \frac{\Gamma_p\left(\frac{\nu+n}{2}\right)}{\pi^{\frac{np}{2}} |\mathbf{I} + \mathbf{X}\boldsymbol{\Psi}^{-1}\mathbf{X}^\top|^{\frac{\nu+n}{2}} |\boldsymbol{\Psi}|^{\frac{n}{2}} \Gamma_p\left(\frac{\nu}{2}\right)},$$

which can help to speed-up computations.

APPENDIX C: PROOFS

C.1. Non-concavity of the log-likelihood. The likelihood function is not log-concave in general. This section analyses the (non)-concavity of the log-likelihood function given in (2.3). More precisely, the following two propositions are proved.

PROPOSITION 1 (Non-concavity in $\boldsymbol{\Psi}$). *For a fixed ν , the log-likelihood function (2.3) is not concave in $\boldsymbol{\Psi}$.*

PROPOSITION 2 (Concavity in ν). *For a fixed positive definite $\boldsymbol{\Psi}$, the log-likelihood function (2.3) is concave in ν .*

Proof of Proposition 1. Assume ν is fixed and consider only the terms involving $\boldsymbol{\Psi}$ in (2.3). We reduce to the one-dimensional case where

$$\ell(\psi) = \frac{k\nu}{2} \log(\psi) - \sum_{i=1}^k \frac{\nu + n_i}{2} \log(\psi + x_i^2),$$

which implies

$$\ell'(\psi) = \frac{k\nu}{2} \frac{1}{\psi} - \sum_{i=1}^k \frac{\nu + n_i}{2} \frac{1}{\psi + x_i^2} \quad \text{and} \quad \ell''(\psi) = -\frac{k\nu}{2} \frac{1}{\psi^2} + \sum_{i=1}^k \frac{\nu + n_i}{2} \frac{1}{(\psi + x_i^2)^2}.$$

It is straightforward to show there exists a value for ψ , n_i and ν for which $\ell''(\psi) > 0$. Since the second derivative is not always negative the log-likelihood ℓ is not log-concave. \square

Proof of Proposition 2. Consider the terms involving ν . Clearly, the mixed terms involving both ν and $\boldsymbol{\Psi}$ are log-linear in ν and hence log-concave. We thus restrict our attention to the remaining terms not dependent on $\boldsymbol{\Psi}$. The sum of these terms are concave in ν , since

$$\log \Gamma_p\left(\frac{\nu + n_i}{2}\right) - \log \Gamma_p\left(\frac{\nu}{2}\right) = \log \frac{\Gamma_p\left(\frac{\nu + n_i}{2}\right)}{\Gamma_p\left(\frac{\nu}{2}\right)} = \sum_{j=1}^p \log \frac{\Gamma\left(\frac{\nu+1-j}{2} + \frac{n_i}{2}\right)}{\Gamma\left(\frac{\nu+1-j}{2}\right)}.$$

which can be seen to be concave since $n_i \geq 1$ for all i and $h(x) = \log\left(\frac{\Gamma(x+a)}{\Gamma(x)}\right)$ is concave for all $x > 0$ and $a > 0$. The concavity of h is easily seen by the fact that $h''(x) = \psi(x+a) - \psi(x) < 0$, where $\psi(\cdot)$ is the tri-gamma function. The tri-gamma function is a well-known monotonically decreasing function. Hence, the likelihood is log-concave in ν . \square

C.2. Existence and uniqueness of likelihood maxima. This section proves Lemmas 1 and 2 which imply Proposition 3.

Before we state the lemmas, the proposition, and their proofs, we see that the reparameterisation of the RCM is irrelevant. Consider the log-likelihood in (2.3) assuming ν fixed. The log-likelihood obey

$$(C.1) \quad 2\ell(\Psi) = c + k\nu \log |\Psi| - \sum_{a=1}^k (n_a + \nu) \log |\Psi + \mathbf{S}_a|.$$

Notice, that this equation also holds in the reparameterization. Here we have

$$\begin{aligned} 2\ell(\Sigma) &= c + k\nu \log |(\nu - p - 1)\Sigma| - \sum_{a=1}^k (n_a + \nu) \log |(\nu - p - 1)\Sigma + \mathbf{S}_a| \\ &= c' + k\nu \log |\Sigma| - \sum_{a=1}^k (n_a + \nu) \log |\Sigma + (\nu - p - 1)^{-1}\mathbf{S}_a|. \end{aligned}$$

Since $(\nu - p - 1)^{-1}\mathbf{S}_a$ is only dependent on data (when ν is fixed) we can set $(\nu - p - 1)^{-1}\mathbf{S}_a := \mathbf{S}_a$. Without loss of generality we can therefore consider (C.1) in the following.

PROPOSITION 3 (Existence and uniqueness). *The log-likelihood (2.3) has a unique maximum in Ψ for fixed ν and $n_\bullet = \sum_{a=1}^k n_a \geq p$.*

Proof of Proposition 3. We first prove existence of the maximum. Note, that we may consider ℓ as a function on a vector space by letting $\Psi = \exp(\mathbf{X})$ where \mathbf{X} is a symmetric matrix. By Lemma 1 and the continuity of ℓ , the set $\{\Psi | \ell(\Psi) \geq \ell(\Psi^*)\}$ is bounded and closed and thus compact for any $\Psi^* \succ 0$. The existence of a maximum follows from the extreme value theorem by the continuity of ℓ . A stationary point exists due to Rolle's theorem and the differentiability of ℓ .

Next, we show the uniqueness of the maximum. Let (\mathcal{ST}) denote the set of stationary points, which is nonempty. By Lemma 1, $\ell(\Psi)$ has a finite upper bound given by the maximum of the log-likelihood in those points. All gradient curves (that is, solution curves to $\dot{\Psi}(t) = \nabla \ell(\Psi(t))$) must then

converge toward exactly one of the stationary points where ℓ monotonically increases along each curve. Define for Ψ_s in \mathcal{ST} the basin of attraction

$$A_s = \{ \Psi_0 \in \mathcal{S}_+ \mid \Psi(0) = \Psi_0, \lim_{t \rightarrow \infty} \Psi(t) = \Psi_s \},$$

The basin of attraction is open if Ψ_s is a maximum (Khalil, 2002, Lemma 4.1). By Lemma 2, Ψ_s is always a maximum and hence all A_s are open sets in the set of all positive definite matrices \mathcal{S}_+ . This partitions the space \mathcal{S}_+ into disjoint, non-empty, open sets. Since \mathcal{S}_+ is connected, this is only possible if $A_s = \mathcal{S}_+$ and thus there is only a single basin of attraction and maximum of ℓ . \square

LEMMA 1. *If there exists an eigenvalue λ_t of Ψ_t such that $\lambda_t \rightarrow 0$ or $\lambda_t \rightarrow \infty$, then $\ell(\Psi_t) \rightarrow -\infty$ for ν fixed and $n_\bullet = \sum_{a=1}^k n_a \geq p$.*

Proof of Lemma 1. Assume the hypothesis of the lemma and consider the expression given in (C.1) up to the addition of a constant. The likelihood obey the following two upper bounds. First,

$$\begin{aligned} \ell(\Psi_t) &= \frac{k\nu}{2} \log |\Psi_t| - \sum_{i=1}^k \frac{\nu + n_i}{2} \log |\Psi_t + \mathbf{S}_i| \\ &\leq \frac{k\nu}{2} \log |\Psi_t| - \sum_{i=1}^k \frac{\nu + n_i}{2} \log |\Psi_t| = -\frac{n_\bullet}{2} \log |\Psi_t| \end{aligned}$$

Secondly, let $C = \sum_{i=1}^k \frac{\nu + n_i}{2} = \frac{k\nu}{2} + \frac{n_\bullet}{2}$, whereby (C.1) can be expressed as

$$\ell(\Psi_t) = \frac{k\nu}{2} \log |\Psi_t| - C \sum_{i=1}^k \frac{\nu + n_i}{2C} \log |\Psi_t + \mathbf{S}_i|.$$

Since $\log |\cdot|$ is concave and the above sum is a convex combination, we have

$$\ell(\Psi_t) \leq \frac{k\nu}{2} \log |\Psi_t| - C \log \left| \Psi_t + \sum_{i=1}^k \frac{\nu + n_i}{2C} \mathbf{S}_i \right|.$$

Hence,

$$\ell(\Psi_t) \leq \min \left\{ -\frac{n_\bullet}{2} a(t), \frac{k\nu}{2} a(t) - C \log |\Psi_t + \mathbf{S}| \right\}$$

where $a(t) = \log |\Psi_t|$ and $\mathbf{S} = \sum_i \frac{\nu+n_i}{2C} \mathbf{S}_i$. Three cases now exists: 1) If $a(t) \rightarrow \infty$, then

$$\ell(\Psi_t) \leq -\frac{n_\bullet}{2} a(t) \rightarrow -\infty.$$

2) If $a(t) \rightarrow -\infty$, then

$$\ell(\Psi_t) \leq \frac{k\nu}{2} a(t) - C \log |\Psi_t + \mathbf{S}| \leq \frac{k\nu}{2} a(t) - C \log |\mathbf{S}| \rightarrow -\infty$$

as the matrix in the second term is almost surely positive definite when $n_\bullet = \sum_{i=1}^k n_a \geq p$ and the log determinant is some constant. 3) If $a(t)$ is bounded and the largest eigenvalue $\lambda_{\max}(\Psi_t) \rightarrow \infty$ (and hence $\lambda_{\min}(\Psi_t) \rightarrow -\infty$), then $\lambda_{\max}(\Psi_t + \mathbf{S}) \rightarrow \infty$ and $\lambda_{\min}(\Psi_t + \mathbf{S})$ is bounded away from zero. Therefore,

$$\ell(\Psi_t) \leq \frac{k\nu}{2} a(t) - C \log |\Psi_t + \mathbf{S}| \rightarrow -\infty,$$

which completes the proof. \square

LEMMA 2. *If $n_\bullet \geq p$ and ν is fixed then the Hessian of the log-likelihood (2.3) is negative definite in all stationary points.*

Proof of Lemma 2. We show the conclusion of the Lemma directly by differentiation of ℓ w.r.t. Ψ . To do so, the matrix cookbook by [Petersen and Pedersen \(2008\)](#) is a useful reference. In particular, see equations (41, p. 8) and (59, p. 9) and pages 14 and 52–53. We first compute expressions for the first and second order derivatives.

First order derivatives. From the log-likelihood expression, we compute the first order derivative $\nabla_{\Psi} 2\ell(\Psi)$ which is the matrix-valued function where each entry is given by

$$(C.2) \quad \frac{\partial 2\ell}{\partial \Psi_{ij}} = k\nu \operatorname{tr}(\mathbf{E}^{ij} \Psi^{-1}) - \sum_{a=1}^k (\nu + n_a) \operatorname{tr}(\mathbf{E}^{ij} (\Psi + \mathbf{S}_a)^{-1}).$$

and \mathbf{E}^{ij} is a matrix with ones at entries (i, j) and (j, i) and zeros elsewhere. This \mathbf{E}^{ij} is introduced as the derivative is not straight-forward because of the symmetric structure of Ψ . Had Ψ been unstructured, then $\frac{\partial}{\partial \Psi} \log |\Psi| = \Psi^{-1}$. However, when Ψ is symmetric we have that $\frac{\partial}{\partial \Psi_{ij}} \log |\Psi| = \operatorname{tr}(\mathbf{E}^{ij} \Psi^{-1})$ which is the same as $\frac{\partial}{\partial \Psi} \log |\Psi| = 2\Psi^{-1} - \Psi^{-1} \circ \mathbf{I}$ where \circ denotes the Hadamard product ([Petersen and Pedersen, 2008](#), eq. (43) and (141)).

The first order derivative lives in a $\binom{p+1}{2}$ -dimensional vector space with basis vectors \mathbf{E}^{ij} indexed by (i, j) , $i \leq j$.

Second order derivatives. We proceed with the second order derivative $\nabla_{\Psi}^2 2\ell(\Psi)$ with entries given by

$$\begin{aligned} \frac{\partial^2 2\ell}{\partial \Psi_{kl} \partial \Psi_{ij}} &= -k\nu \operatorname{tr}\left(\mathbf{E}^{ij} \Psi^{-1} \mathbf{E}^{kl} \Psi^{-1}\right) \\ &\quad + \sum_{a=1}^k (\nu + n_a) \operatorname{tr}\left(\mathbf{E}^{ij} (\Psi + \mathbf{S}_a)^{-1} \mathbf{E}^{kl} (\Psi + \mathbf{S}_a)^{-1}\right), \end{aligned}$$

obtained by differentiation of (C.2) using $\frac{\partial}{\partial \Psi_{ij}} \Psi^{-1} = -\Psi^{-1} \mathbf{E}^{ij} \Psi^{-1}$ (Petersen and Pedersen, 2008, eq. (40)) and the linearity of the trace operator.

The second order derivative is a $\binom{p+1}{2} \times \binom{p+1}{2}$ -dimensional matrix indexed by (i, j) and (k, l) , $i \leq j$, $k \leq l$.

Negative definiteness of stationary points. With the above expressions we now show that the Hessian matrix is negative definite in all stationary points. Let $\mathbf{Y} = \sum_{(i,j)} y_{ij} \mathbf{E}^{ij}$ be an arbitrary symmetric matrix in the vector space where $\mathbf{Y} \neq \mathbf{0}$. In our vector space we need to show that

$$\sum_{i \leq j, k \leq l} Y_{ij} (\nabla_{\Psi}^2 2\ell(\Psi))_{(i,j),(k,l)} Y_{kl} < 0$$

holds in every stationary point analogous to $\mathbf{z}^\top \mathbf{A} \mathbf{z} = \sum_{ij} A_{ij} z_i z_j < 0$. From the second derivative, this amounts to showing that in every stationary point,

(C.3)

$$-k\nu \operatorname{tr}(\mathbf{Y} \Psi^{-1} \mathbf{Y} \Psi^{-1}) + \sum_{a=1}^k (\nu + n_a) \operatorname{tr}\left(\mathbf{Y} (\Psi + \mathbf{S}_a)^{-1} \mathbf{Y} (\Psi + \mathbf{S}_a)^{-1}\right) < 0.$$

Now, by the positive-definiteness of Ψ , let

$$\begin{aligned} \mathbf{Y} &:= \Psi^{-\frac{1}{2}} \mathbf{Y} \Psi^{-\frac{1}{2}} \text{ and} \\ \mathbf{S}_a &:= \Psi^{-\frac{1}{2}} \mathbf{S}_a \Psi^{-\frac{1}{2}}, \end{aligned}$$

and thus without loss of generality we can assume that $\Psi = \mathbf{I}$. Hence, the derivative of the likelihood (C.2) equated to zero, becomes

$$k\nu \mathbf{I} = \sum_a (n_a + \nu) (\mathbf{I} + \mathbf{S}_a)^{-1}$$

which implies (by multiplication by \mathbf{Y} on each side) that every stationary point obey

$$(C.4) \quad k\nu \operatorname{tr}(\mathbf{Y}^2) = \sum_a (n_a + \nu) \operatorname{tr}(\mathbf{Y}(\mathbf{I} + \mathbf{S}_a)^{-1}\mathbf{Y}).$$

We substitute (C.4) into (C.3) to get

$$\begin{aligned} & \sum_a (n_a + \nu) \operatorname{tr}(\mathbf{Y}(\mathbf{I} + \mathbf{S}_a)^{-1}\mathbf{Y}(\mathbf{I} + \mathbf{S}_a)^{-1} - \mathbf{Y}(\mathbf{I} + \mathbf{S}_a)^{-1}\mathbf{Y}) \\ &= \sum_a (n_a + \nu) \operatorname{tr}(\mathbf{Y}(\mathbf{I} + \mathbf{S}_a)^{-1}\mathbf{Y}[(\mathbf{I} + \mathbf{S}_a)^{-1} - \mathbf{I}]) < 0. \end{aligned}$$

We note that $\mathbf{S}_a = \mathbf{X}_a\mathbf{X}_a^\top$ and

$$(\mathbf{I} + \mathbf{S}_a)^{-1} - \mathbf{I} = -\mathbf{X}_a(\mathbf{I} + \mathbf{X}_a^\top\mathbf{X}_a)^{-1}\mathbf{X}_a^\top,$$

by the matrix inversion lemma whereby we need to show that

$$\sum_a (n_a + \nu) \operatorname{tr}(\mathbf{Y}(\mathbf{I} + \mathbf{X}_a\mathbf{X}_a^\top)^{-1}\mathbf{Y}\mathbf{X}_a(\mathbf{I} + \mathbf{X}_a^\top\mathbf{X}_a)^{-1}\mathbf{X}_a^\top) > 0.$$

Assume that the sum is actually zero. Since $(\mathbf{I} + \mathbf{X}_a\mathbf{X}_a^\top)^{-1} \succ 0$ we then obtain that

$$\mathbf{Y}\mathbf{X}_a(\mathbf{I} + \mathbf{X}_a\mathbf{X}_a^\top)^{-1}\mathbf{X}_a^\top\mathbf{Y} = 0 \quad \text{for } a = 1, \dots, k.$$

Again by $(\mathbf{I} + \mathbf{X}_a\mathbf{X}_a^\top)^{-1} \succ 0$ we conclude that $\mathbf{Y}\mathbf{X}_a = 0$ for all $a = 1, \dots, k$, i.e. $\mathbf{Y}(\mathbf{X}_1, \dots, \mathbf{X}_k) = 0$. If $n_\bullet \geq p$ then almost surely $(\mathbf{X}_1, \dots, \mathbf{X}_k)$ has rank p whereby $\mathbf{Y} = 0$. \square

APPENDIX D: LIKELIHOOD OF THE PRECISION MATRIX

Suppose we have k i.i.d. realizations, $\mathbf{\Delta}_1, \dots, \mathbf{\Delta}_k$, from the Wishart distribution given in model (2.5). The corresponding log-likelihood can be computed straight-forwardly:

$$\begin{aligned} \ell(\mathbf{\Theta}|\mathbf{\Delta}_1, \dots, \mathbf{\Delta}_k) &= \sum_{i=1}^k \log \frac{|\mathbf{\Theta}|^{-\frac{\nu}{2}}}{2^{-\frac{\nu p}{2}} \Gamma_p(\frac{\nu}{2})} |\mathbf{\Delta}_i|^{\frac{\nu-p-1}{2}} e^{-\frac{1}{2} \operatorname{tr}(\mathbf{\Theta}^{-1}\mathbf{\Delta}_i)} \\ &= c + \sum_{i=1}^k \left(-\frac{\nu}{2} \log |\mathbf{\Theta}| - \frac{1}{2} \operatorname{tr}(\mathbf{\Theta}^{-1}\mathbf{\Delta}_i) \right) \\ &= c - \frac{\nu k}{2} \left(\log |\mathbf{\Theta}| + \operatorname{tr} \left(\mathbf{\Theta}^{-1} \frac{1}{\nu k} \sum_{i=1}^k \mathbf{\Delta}_i \right) \right). \end{aligned}$$

The last expression is to be maximized with respect to Θ and can be recognized as the MLE problem in a multivariate Gaussian distribution. Hence, $\Theta = \frac{1}{k\nu} \sum_{i=1}^k \Delta_i$, is the MLE in this model.

APPENDIX E: APPROXIMATE MLE

To find the maximizing parameters we differentiate (2.3) w.r.t. Ψ and equate to zero while assuming ν known and constant. The first order derivative can be seen in equation (C.2). Equating to zero yields

$$\begin{aligned} \mathbf{0} &= \frac{k\nu}{2} \Psi^{-1} - \sum_{i=1}^k \frac{\nu + n_i}{2} (\Psi + \mathbf{S}'_i)^{-1} \\ &= \frac{k\nu}{2} \Psi^{-1} - \sum_{i=1}^k \frac{\nu + n_i}{2} (\mathbf{I} + \Psi^{-1} \mathbf{S}_i)^{-1} \Psi^{-1}. \end{aligned} \quad (\text{E.1})$$

This implies $k\nu \mathbf{I} - \sum_{i=1}^k (\nu + n_i) (\mathbf{I} - (-\Psi^{-1} \mathbf{S}_i))^{-1} = \mathbf{0}$ which can be rewritten as

$$k\nu \mathbf{I} - \sum_{i=1}^k (\nu + n_i) \sum_{l=0}^{\infty} (-\Psi^{-1} \mathbf{S}_i)^l = \mathbf{0},$$

by the Neumann series $((\mathbf{I} + \mathbf{A})^{-1} = \sum_{l=0}^{\infty} \mathbf{A}^l)$ provided that $\lim_{l \rightarrow \infty} (\mathbf{I} - \Psi^{-1} \mathbf{S}_i)^l = \mathbf{0}$ for all i . This holds if the eigenvalues of $\Psi^{-1} \mathbf{S}_i$ are less than 1. We approximate by the first order expansion ($l = 1$), and

$$\mathbf{0} = k\nu \mathbf{I} - \sum_{i=1}^k (\nu + n_i) (\mathbf{I} - \Psi^{-1} \mathbf{S}_i) = -n_{\bullet} \mathbf{I} + \Psi^{-1} \sum_{i=1}^k (\nu + n_i) \mathbf{S}_i$$

where $n_{\bullet} = \sum_{i=1}^k n_i$ is the total number of observations. This implies

$$\Psi^{-1} \sum_{i=1}^k (\nu + n_i) \mathbf{S}_i = n_{\bullet} \mathbf{I}$$

which suggests the estimators

$$\hat{\Psi}_{\text{MLE}} = \frac{\sum_{i=1}^k (\nu + n_i) \mathbf{S}_i}{n_{\bullet}} \quad \text{and} \quad \hat{\Sigma}_{\text{MLE}} = \frac{\sum_{i=1}^k (\nu + n_i) \mathbf{S}_i}{(\nu - p - 1)n_{\bullet}}. \quad (\text{E.2})$$

These estimates are seen to correspond to a weighted sum of the scatter matrices.

APPENDIX F: DERIVATION OF ICC

Consider observations from (2.1). We temporarily abuse our notation and let

$$\boldsymbol{\Sigma} \sim \mathcal{W}_p^{-1}(\boldsymbol{\Psi}, \nu) \quad \text{and} \quad \mathbf{S}|\boldsymbol{\Sigma} \sim \mathcal{W}_p(\boldsymbol{\Sigma}, 1),$$

and consider only a single observation ($n = 1$). Furthermore, let $\mathbf{S} = (S_{ij})_{p \times p}$, $\boldsymbol{\Sigma} = (\Sigma_{ij})_{p \times p}$, and $\boldsymbol{\Psi} = (\Psi_{ij})_{p \times p}$. To compute the ICC, we are thus interested in the ratio of the quantities $\text{Var}(\Sigma_{ij})$ and $\text{Var}(S_{ij})$ corresponding to the between-study and total variation of the covariance between variables i and j , respectively. That is, the ICC is the proportion of the total variance between studies,

$$(F.1) \quad \text{ICC}(\nu) = \frac{\text{Var}(\Sigma_{ij})}{\text{Var}(S_{ij})} = \frac{\text{Var}(\Sigma_{ij})}{\text{Var}(\Sigma_{ij}) + \mathbb{E}[\text{Var}(S_{ij}|\boldsymbol{\Sigma})]},$$

where the second equality is obtained by $\mathbb{E}[S_{ij}|\boldsymbol{\Sigma}] = \Sigma_{ij}$ and the law of total variation. This equality agrees with the usual ICC as $\mathbb{E}[\text{Var}(S_{ij}|\boldsymbol{\Sigma}_{ij})]$ can be interpreted as the (expected) within-study variation. Using the conditional variance given by $\text{Var}(S_{ij}|\boldsymbol{\Sigma}) = \Sigma_{ij}^2 + \Sigma_{ii}\Sigma_{jj}$ the needed quantities can be found. To compute an expression for (F.1) we need to consider the fourth-order moments of the observations. From the model, known results of the inverse Wishart distribution, cf. (Cook and Forzani, 2011; von Rosen, 1988), leads to

$$(F.2) \quad \text{Cov}(\Sigma_{ij}, \Sigma_{kl}) = \frac{2\Psi_{ij}\Psi_{kl} + (\nu - p - 1)(\Psi_{ik}\Psi_{jl} + \Psi_{il}\Psi_{kj})}{(\nu - p)(\nu - p - 1)^2(\nu - p - 3)}, \quad \nu > p + 3,$$

implying that

$$(F.3) \quad \text{Var}(\Sigma_{ij}) = \text{Cov}(\Sigma_{ij}, \Sigma_{ij}) = \frac{(\nu - p + 1)\Psi_{ij}^2 + (\nu - p - 1)\Psi_{ii}\Psi_{jj}}{(\nu - p)(\nu - p - 1)^2(\nu - p - 3)}.$$

Continuing with the expected conditional variance of $S_{ij}|\boldsymbol{\Sigma}$ in the denominator of (F.1),

$$(F.4) \quad \begin{aligned} \mathbb{E}[\text{Var}(S_{ij}|\boldsymbol{\Sigma}_{ij})] &= \text{Var}(\Sigma_{ij}) + \mathbb{E}[\Sigma_{ij}^2] + \text{Cov}(\Sigma_{ii}, \Sigma_{jj}) + \mathbb{E}[\Sigma_{ii}]\mathbb{E}[\Sigma_{jj}] \\ &= \text{Var}(\Sigma_{ij}) + \text{Cov}(\Sigma_{ii}, \Sigma_{jj}) + (\nu - p - 1)^{-2}(\Psi_{ij}^2 + \Psi_{ii}\Psi_{jj}). \end{aligned}$$

An expression of $\text{Var}(S_{ij})$ in terms of the elements of $\boldsymbol{\Psi}$ can then found by substituting (F.2) and (F.3) into (F.4) and by extension an expression for the ICC (F.1) can be obtained. We omit this tedious calculation which can be verified to yield $\text{ICC}(\nu) = 1/(\nu - p)$ as given in (2.7)

DEPARTMENT OF HAEMATOLOGY
SDR. SKOVVEJ 15
DK-9000 AALBORG
E-MAIL: anders.ellern.bilgrau@gmail.com
rfb@rn.dk
mboegsted@dcm.aau.dk
k.dybkaer@rn.dk

DEPARTMENT OF MATHEMATICAL SCIENCES
FREDRIK BAJERS VEJ 7G
DK-9220 AALBORG Ø
E-MAIL: anders.ellern.bilgrau@gmail.com
svante@math.aau.dk

DEPARTMENT OF CLINICAL MEDICINE
SDR. SKOVVEJ 15
DK-9000 AALBORG Ø
E-MAIL: mboegsted@dcm.aau.dk
k.dybkaer@rn.dk